

Determination of Preferred Fiber Orientation State based on Newton – Raphson Method using on Exact Jacobian

Aigbe Awenlimobor *, Douglas E. Smith

Department of Mechanical Engineering, School of Engineering and Computer Science, Baylor University, Waco, TX 76798, USA

*Corresponding author. Email: aigbe_awenlimobor1@baylor.edu

Abstract

Fiber orientation is an important descriptor of the intrinsic microstructure of polymer composite materials and the ability to predict the orientation state accurately and efficiently is crucial in evaluating the bulk thermo-mechanical behavior and consequently performance of printed part. Recent macroscopic fiber orientation models have employed the moment-tensor form in representing the fiber orientation state thus requiring some form of closure approximation of a higher order orientation tensor. Currently, different models have been developed to account for the added effect of rotary diffusion due to fiber-fiber and fiber-matrix interactions and accurately simulate the experimentally observed slow fiber kinematics in polymer composite processing. Traditionally explicit numerical IVP-ODE transient solvers like the 4th order Runge-Kutta method has been used to determine the steady-state fiber orientation. Here we propose a computationally efficient and faster method based on Newton-Raphson iterative technique for determining the preferred orientation state by evaluating the exact derivatives of the moment-tensor evolution equation with respect to the independent components of the orientation tensor. We consider various existing macroscopic-fiber orientation models and different closure approximations to ensure to ensure the robustness and reliability of the method, and we evaluate its performance and stability in determining physical solutions in various complex flow fields. Validation of the obtained exact partial derivatives of the material derivative of the orientation tensor is carried out by benchmarking with results of finite difference techniques.

Introduction

Mechanical performance of printed parts depends on the inherent process-induced microstructural properties. Of the different bead microstructure descriptors for fiber reinforced composite polymer, the fiber orientation is a key parameter useful in material behavior prediction. As such, appropriate macroscopic modelling of the average fiber orientation distribution is crucial in predicting these properties. Pioneering work by Jeffery [1] for describing the evolution of a single rigid ellipsoid fiber in viscous flow of a suspension with Newtonian property based on linearization of the Navier Stokes equation forms the basis for most model development. The Jeffery's hydrodynamic (HD) model is limited to dilute suspension and ignores the effect of Brownian disturbance and momentum diffusion due to fiber-fiber interactions. Moreover, Jeffery's assumption also ignores the flexural and fracture behavior of the fiber and assumes no slippage contact between the fiber and surrounding fluid. Studies have shown that fibers ultimately tend to orient themselves relative to the flow field [2]. Various improvements to the Jeffery's single fiber model have been made to model the bulk behavior of fibers in semi-dilute and concentrated suspension due to fiber-fiber interaction. Although theoretically feasible, it is computationally expensive and impractical to simulate the behavior of every individual particle in the fiber suspension flow. Folgar and Tucker [3, 4] introduced a phenomenological isotropic rotary diffusion (IRD) term with a linear dependence on the scalar

magnitude of the rate of deformation tensor and based on an orientation probability distribution function (ODF) in addition to the hydrodynamic contribution from Jeffery's model. The time evolution of the ODF is defined by the Fokker-Plank equation for probability distribution function (PDF) of fiber orientation. Conventionally a numerical method such as finite volume (cf. Bay [5]) and more recently a more computationally efficient exact spherical harmonics method (cf. Montgomery-Smith et. al [6]) has been used to solve the Folgar-Tuckers (FT) equation of change for fiber orientation, but the advent of tensorial representation of the orientation evolution based on series expansion of even order moments of the fiber orientation PDF by Advani and Tucker [7], further served to simplify the more complicated ODF – FT model. The Advani-Tucker's n^{th} order orientation evolution model is less accurate depending on the order of the tensor and thus requires a closure approximation. Due to experimentally observed disparity in the fiber orientation kinetics compared to those computed from traditional orientation models, different model corrections have been proposed to retard the evolution rate. Huynh [8] applied a strain retarding factor (SRF) to the Advani-Tucker's model to slow down the evolution speed. Huynh's SRF model lacked material objectivity. To address the non-objectivity of Huynh's model, Wang et al. [9] developed a phenomenological reduced strain closure (RSC) model that applies the reduction factor solely to the spectral decomposed principal rates of the orientation tensor, without modifying the evolution of the rotation tensor. Similarly, Tseng et. al [10, 11] proposed a retarding principal rate (RPR) model that involved a coaxial correction to the FT model by assuming the intrinsic orientation kinetics (IOK) describing the behavior of the fiber suspension involved a nonlinear modification to the principal directions of the material derivative. Prediction of fiber orientation based on IRD models have been experimentally observed to be valid only for short-fiber/thermoplastic composites (SFT), with fiber length typically in the range of 0.2mm to 0.4mm [12]. For long-fiber/thermoplastic composites (LFT) with typical size between 10mm to 13mm, the IRD models possess unidirectional prediction effectiveness. Different researchers have proposed models that involves modifying the rotary diffusion term for an all-round competency in accurately predicting the components of the orientation tensor. Ranganathan et al [13] assumed an isotropic rotary diffusivity that inversely varies with the degree of alignment of the orientation tensor with a phenomenological interaction parameter that depends on the reciprocal of the inter fiber spacing. Their model application was limited to the transient orientation state and suited for long range fiber-fiber interaction. Their model was however unsuitable for LFTs steady state orientation prediction as with other IRD models since its diffusivity was isotropic. Fan et al. [14] and Phan-Thien [15], were the first to propose an anisotropic rotary diffusion (ARD) moment-tensor model by substituting the scalar phenomenological interaction parameter with a second order anisotropic rotary diffusion tensor. Their model was however exclusive and restricted in application. At the same time, Koch [16] developed an ARD model suited for semi-dilute suspension with an anisotropic spatial diffusion tensor that depends on the orientation state and the rate of deformation tensor. However, their model was based on the more complicated PDF form for the orientation tensor representation rather than the moment-tensor form and proved ineffective in LFT modelling. Phelps et. al [12] built on the work of Fan [14] and Phan-Thien et al [15] and developed a more general moment-tensor anisotropic diffusion model that depends on the spatial diffusion tensor and orientation tensor state. The derivation of the spatial diffusion tensor was based on similar representation by Hand [17] as a function of the orientation state and rate of deformation tensor. Phelps's model had remarkable improvements in predicting orientation state of LFTs. Tseng et al. [18] proposed an improved anisotropic rotary diffusion model (iARD) which defines a two-parameter spatial diffusion tensor model that couples the effect of fiber-matrix interaction and fiber-fiber interaction. The iARD model fell short in terms of material non-objectivity. Recently, Tseng et. al [19] proposed a principal anisotropic rotary diffusion (pARD) model that assumes a principal spatial diffusion tensor that corotates with the orientation tensor. Bakharev A. [20] proposed a moldflow rotational diffusion (MRD) model based on reduction of the terms of the generic ARD model by Phelps to just linear terms with a spatial diffusion tensor like Tseng's model. Latz et al [21]

developed a fully coupled flow-orientation model for concentrated suspensions by replacing the diffusion term in the FT model with an effective collision tensor that incorporates both isotropic diffusion interaction term and a topological exclusion interaction term based on a nematic (NEM) ‘Onsager’ potential of non-Brownian Maier-Saupe form. They found the influence of the topological interaction on the fiber orientation state to be flow dependent having significant effect on channel and contraction flow with relatively lesser influence on flow around cylinder. Kugler et al [22], Favaloro et al. [23], Agboola et al. [24] and Park et al. [25] presents detailed review and comparison of existing fiber orientation models. The foregoing ARD models find useful application in polymer composite industry and have been incorporated in mold-filling flow computations in injection molding process simulations [26,27,28,29,30,31,32].

Due to the absence of exact solutions for orientation state for inhomogeneous flows involving momentum diffusion, various closure approximations with different degree of accuracy have been developed for higher orders of the moment-tensor fiber orientation equation. Hand G.L [17] first proposed the linear (LIN) closure based on a linear combination of terms of the 2nd order orientation tensor and identity matrix. Doi [33] and Lipscomb et al. [34] introduced the quadratic (QDR) closure of a higher order tensor which is formed from dyadic products of lower order tensors. The QDR closure inherently lacks symmetry property requirement but preserves the symmetry of the computed lower order tensor. The LIN closures are exact for random orientation distribution while the QDR closures are exact for uniaxially aligned fiber orientation. Advani and Tucker [7] developed a hybrid closure which is a weighted sum of both the LIN and QDR closure approximations where they defined the weighting factor as an invariant of the orientation state. Expectedly they found the hybrid model to perform better for transient state orientation prediction. The hybrid closure however tends to over-predict the orientation tensor compared with the more accurate distribution function closure (DFC). DFC are however computationally involved since they require finite difference grid in space and time. Hinch and Leal [35] developed numerous composite closure approximations for the 4th order tensor in precontracted forms with the deformation rate tensor and the accuracy of their predictions were dependent on flow selective and dependent on flow strength. Recently, more accurate higher order polynomial closure approximations have been developed including the eigenvalue-based fitting (EBF) that involves principal axis transformation and the Invariant-based fitting (IBF). The orthotropic smooth (ORS), orthotropic fitted (ORF) closures and ORF closures for low fiber-fiber interaction coefficient (ORL) fall under the class of EBF closures and were developed by Cintra and Tucker [36] based on the assumption of coincident principal axis of the 2nd and 4th order tensor. The ORF independent coefficients are derived from a 2nd order polynomial fit of the principal axis data obtained from DFC via a minimization technique. The ORF had better performance compared to non-fitted closure approximations however the ORF behaved poorly for flows with very low interaction coefficients and sometimes gave non-physical oscillations like the behavior of the Hinch and Leal closure (HL2) in same condition. Though the ORL behaves better for low interaction coefficient in simple shear flow yet overpredicts the flow direction orientation tensor and is unstable for radial diverging flows. Chung and Kwon [37,38], improved the ORF and developed the 2nd order ORW and 3rd order polynomial ORW3 closures for wide interaction coefficients that is stable for all flow conditions using new flow data from distribution function calculation (DFC). Kuzmin D [39] presents details on derivations of some orthotropic fitted closures via a numerical bottom top approach. Recently the eigenvalue-based optimal fitting (EBOF) closures were developed which are extensions to the ORF but with higher order polynomial fits for improved accuracy such as the 4th order polynomial fitted closure by Verwyst [40] (ORT) and rational elliptical (RE) closure by Wetzel [41] using Carlson elliptical integrals. Mullens et al. [42] developed several high order polynomials fitted closures for short fiber composites and introduced the time derivative fitted closures. Of the class of IBF closures, the natural (NAT) closure approximation of Verleye and Dupret [43] was built on the work of Lipscomb et al. [34] and formed the basis of other IBF developments. They

developed a general expression for the full symmetric 4th order tensor in terms of the 2nd order tensor, the identity matrix and fitted coefficients as functions of the tensor invariant which were derived from analytical calculations based on a least square fitting process. The NAT closure assumed the absence of fiber-fiber interaction and infinitely long fiber geometry. The closure is exact based on the foregoing assumptions however it has been reported to possess singularities for axisymmetric orientation states. The Invariant based optimal fitting (IBOF) closure developed by Chung and Kwon [44] was an extension to the NAT closure development however the independent coefficients are derived from regression analysis based on actual data obtained from DFC considering different flow types like EBF closures. EBF closures are computationally more involved in numerical calculations of actual flows compared with the IBF closures because of the principal axis transformation. Other highly accurate closure approximations include the neural network based fitted closures by Jack et al [45] and the 6th order Invariant based orthotropic fitted closure by Jack and Smith [46,47].

The steady state orientation tensor values have traditionally been computed with time evolution numerical IVP-ODE techniques like the famous 4th order Runge-Kutta method or predictor-corrector methods. Here we present a computationally efficient and faster method based on Newton Raphson algorithm for determining the steady state or preferred orientation using explicit derivatives of the 2nd order tensor equation of change with respect to its orientation tensor components for different macroscopic fiber orientation models considering various closure approximations and their performance in complex flow fields. We benchmark results of the explicit derivatives with those obtained using finite differences to ensure accuracy. The explicit derivatives are comparatively faster compared to the finite difference derivatives.

Methodology

Determination of Preferred Orientation

The focus of this paper is to develop a numerical based approach in determining the steady state orientation vector p_i or tensor a_{ij} that results in zero rate of change of the orientation state by employing the iterative numerical Newton Raphson algorithm, setting the rate of change equation or residual to zero. i.e.,

$$R_i = \frac{Dp_i}{Dt} = 0, \quad R_{ij} = \frac{Da_{ij}}{Dt} = 0 \quad 1$$

based on Newton's algorithm, the successive iterative improvement to the approximation of a given root (in our case the orientation state) is given as [48]

$$p_i^+ = p_i^- - J_{ij}^{-1} R_j \quad 2$$

and for the 2nd order tensor

$$a_{ij}^+ = a_{ij}^- - J_{mnij}^{-1} R_{mn}^- \quad 3$$

The implication of this is the need to determine explicit derivatives for the time rate of change of the orientation tensor/vector with respect to its components to obtain the Jacobian. i.e.

$$J_{ij} = \frac{\partial R_i}{\partial p_j}, \quad J_{mnij} = \frac{\partial R_{mn}}{\partial a_{ij}} \quad 4$$

In the succeeding sections, we present various existing models for rate of change equation of the orientation tensor based on a review by Kugler et al. [22] representing the residual and we derive the associated Jacobian for each model.

Fiber Orientation

The orientation state of any fiber can be described by a probability distribution function (PDF) $\psi(\underline{p})$ of all the possible directions of \underline{p} where \underline{p} is the unit vector associated with the fiber given as [7]

$$\underline{p} = \begin{bmatrix} \sin \theta \cos \phi \\ \sin \theta \sin \phi \\ \cos \theta \end{bmatrix} \quad 5$$

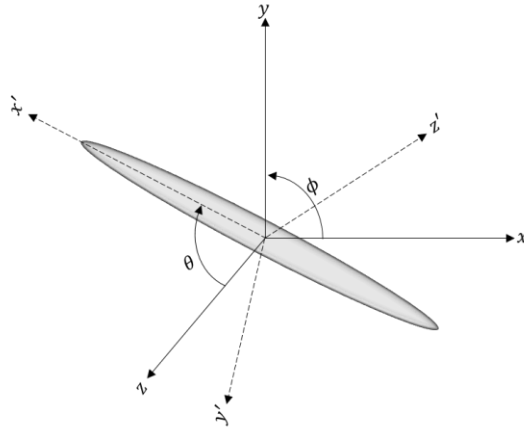


Figure 1 : Single 'rigid' ellipsoidal fiber orientation

$\psi(\underline{p})$ is periodic i.e., $\psi(\underline{p}) = \psi(-\underline{p})$ and satisfies the normalization condition.

$$\oint \psi(\underline{p}) d\underline{p} = \int_{\theta=0}^{\pi} \int_{\phi=0}^{2\pi} \psi(\theta, \phi) \sin \theta d\theta d\phi = 1 \quad 6$$

The PDF satisfies the continuity condition [7]

$$\frac{D\psi}{Dt} = -\frac{\partial}{\partial \underline{p}}(\psi \dot{\underline{p}}) \quad 7$$

Macroscopic Fiber Orientation Modelling

Macroscopic fiber Orientation modelling is usually required in polymers processing to predict the bulk response of chopped fibers in composites parts and ultimately determine part performance. The choice of macroscopic model depends on various processing parameters such as the concentration of fiber suspension, flow type and strength, fiber geometry and volume fraction, material rheology, etc. Fiber suspension concentration are classified into 3 regimes depending on the fiber volume fraction $\phi_f = nV_f$, n is the number of fibers per unit volume and V_f is the fiber volume. Depending on the degree of fiber alignment and fiber's length, the various suspension regimes are [47,49,50]

$$\begin{cases} \phi_f < \frac{1}{r_e^2}, & \text{dilute} \\ \frac{1}{r_e^2} \leq \phi_f < \frac{1}{r_e}, & \text{semi-concentrated} \\ \phi_f \geq \frac{1}{r_e}, & \text{concentrated} \end{cases} \quad 8$$

Macroscopic Fiber Orientation Model in Dilute Regime

The Jeffery's hydrodynamic model for the motion of a single rigid ellipsoidal particle in incompressible, Newtonian viscous suspension forms the basis for fiber orientation determination in dilute suspension. Jeffery assumed that the particle is advected with bulk motion of the undisturbed surrounding fluid. Jeffery's model is valid for a particle whose linear dimensions multiplied by its velocity pales in comparison to the kinematic viscosity of the fluid. The equation describing Jeffery's motion is given by [1,22,23].

$$\dot{p}_i^{JF} = \omega_{ij}p_j + \xi(\dot{\gamma}_{ij}p_j - \dot{\gamma}_{kl}p_kp_l p_i) \quad 9$$

Where, ω_{ij} and $\dot{\gamma}_{ij}$ are the anti-symmetric and symmetric decomposition of the deformation rate tensor $L_{ij} = \partial v_i / \partial x_j$ and can be given respectively as

$$\omega_{ij} = \frac{1}{2} \left(\frac{\partial v_i}{\partial x_j} - \frac{\partial v_j}{\partial x_i} \right), \quad \dot{\gamma}_{ij} = \frac{1}{2} \left(\frac{\partial v_i}{\partial x_j} + \frac{\partial v_j}{\partial x_i} \right) \quad 10$$

Such that $L_{ij} = \partial v_i / \partial x_j = \dot{\gamma}_{ij} + \omega_{ij}$, ξ is a particle shape parameter given as $\xi = (r_e^2 - 1) / (r_e^2 + 1)$, r_e is the geometric aspect ratio of the particle.

The Newton Raphson residual R_i for Newtons model is thus:

$$R_i^{JF} = \dot{p}_i^{JF}$$

The Jacobian is obtained by taking derivatives with respect to the components of p_i , i.e.

$$J_{mn}^{JF} = \frac{\partial \dot{p}_m^{JF}}{\partial p_n} = \omega_{mj}\delta_{jn} + \xi[\dot{\gamma}_{mj}\delta_{jn} - \dot{\gamma}_{kl}(\delta_{kn}p_l p_m + p_k \delta_{ln} p_m + p_k p_l \delta_{mn})] \quad 11$$

Noting that the derivative of the orientation vector with respect to its individual components is the identity matrix, i.e., $\partial p_i / \partial p_j = \delta_{ij}$. There are only 2 independent components of the orientation vector, i.e., R_i^{JF} is a 2×1 vector. Thus J_{mn}^{JF} is a 2×2 matrix. Jeffery's model has limited application because the polymer melt in the actual injection molding process is non-Newtonian and the fiber's flexural and fracture properties are significant in contrast with Jefferies model assumption. Moreover, Jeffery's model ignores the effect due to fiber-fiber interaction, hence more elaborate models have been developed by researchers to capture these effects.

Macroscopic Fiber Orientation Model in Concentrated Regime

1. The Folgar-Tucker model

The effect of momentum diffusion due to short- and long-range fiber-fiber interaction are accounted for in suspension models in concentrated regime. The Folgar-Tucker model [3,4] was among the earlier models

to account for this phenomenon by incorporating a diffusion term to Jeffery's single fiber model, given thus.

$$\dot{p}_i^{FT} = \dot{p}_i^{JF} - D_r \frac{1}{\psi} \frac{\partial \psi}{\partial p_i} \quad 12$$

Where D_r is the rotary diffusivity term and a constant value account for the Brownian effect of very fine particles. For slender long particles $\xi \approx 1$, Folgar and Tucker suggested a relation for D_r i.e., $D_r = C_I \dot{\gamma}$, where C_I is a phenomenological interaction coefficient and $\dot{\gamma}$ is the scalar magnitude of the strain rate tensor $\dot{\gamma}_{ij}$ given as

$$\dot{\gamma} = \sqrt{2\dot{\gamma}_{ij}\dot{\gamma}_{ji}} \quad 13$$

The PDF ψ defines the probability of a given fiber in a particular orientation state and the rate of change of ψ is given by the Fokker-Planck's continuity equation describing its time evolution.

$$\frac{D\psi}{Dt} = -\frac{\partial}{\partial p_i} (\psi \dot{p}_i) \quad 14$$

The PDF form of Folger-Tuckers model presented itself as a complicated and computationally intensive problem which made it difficult to use. Advani and Tucker [7] presented a simplified moment-tensor form to Folger-Tuckers model by defining a set of even order orientation tensors as integral products of the orientation vector \underline{p} with the PDF ψ over the surface of a unit sphere. For the 2nd and 4th order tensor, these is respectively given as

$$\begin{aligned} a_{ij} &= \oint p_i p_j \psi(\underline{p}) d\underline{p} \\ a_{ijkl} &= \oint p_i p_j p_k p_l \psi(\underline{p}) d\underline{p} \end{aligned} \quad 15$$

The tensors defined in this form are completely symmetric i.e.

$$\begin{aligned} a_{ij} &= a_{ji} \\ a_{ijkl} &= a_{jikl} = a_{kijl} = a_{ljk i} = a_{ilkj} = \dots, \quad 24 \text{ permutations} \end{aligned}$$

And based on the normalization condition of equation xx, the following tensor properties were obtained.

$$a_{ii} = 1, \quad a_{ijkk} = a_{ij}$$

Consequently, there are only 5 independent components of the 9 components of the 2nd order tensor and 9 independent components of the 81 components of the 4th order tensor. The rest can be derived based on the above tensor properties. With this definition, Advani and Tucker developed an equation of change the 2nd order orientation tensors in terms of the 2nd and 4th order tensor thus.

$$\frac{Da_{ij}}{Dt} = \dot{a}_{ij}^{FT} = \{\dot{a}_{ij}^{HD} + \dot{a}_{ij}^{RD}\} \quad 16$$

\dot{a}_{ij}^{HD} is the hydrodynamic tensor component of the Folger-Tuckers that represents Jeffery's equation and given as

$$\dot{a}_{ij}^{HD} = -(\omega_{ik} a_{kj} - a_{ik} \omega_{kj}) + \xi(\dot{\gamma}_{ik} a_{kj} - a_{ik} \dot{\gamma}_{kj} - 2\dot{\gamma}_{kl} a_{ijkl}) \quad 17$$

And \dot{a}_{mn}^{IRD} is the isotropic rotary diffusion term modelling fiber interaction and is given as

$$\dot{a}_{ij}^{IRD} = 2D_r(\delta_{ij} - \alpha a_{ij}) \quad 18$$

α is a dimension factor, $\alpha = 3$ for 3D orientation and $\alpha = 2$ for 2D planar orientation. The residual for the Folger-Tuckers model is thus.

$$R_{mn}^{FT} = \dot{a}_{ij}^{FT} \quad 19$$

The associated Jacobian J_{mnij}^{FT} is obtained by differentiating the residual with-respect-to components of the 2nd order orientation tensor a_{ij} thus.

$$J_{mnij}^{FT} = \frac{\partial R_{mn}^{FT}}{\partial a_{ij}} = \frac{\partial \dot{a}_{mn}^{HD}}{\partial a_{ij}} + \frac{\partial \dot{a}_{mn}^{IRD}}{\partial a_{ij}} \quad 20$$

The derivative of the 2nd order orientation tensor with respect to its individual components is simply

$$\frac{\partial a_{mn}}{\partial a_{ij}} = \delta_{mi}\delta_{nj} \quad 21$$

where,

$$\frac{\partial \dot{a}_{mn}^{HD}}{\partial a_{ij}} = (-\omega_{mk} + \xi \dot{\gamma}_{mk})\delta_{ki}\delta_{nj} + (\omega_{kn} + \xi \dot{\gamma}_{kn})\delta_{mi}\delta_{kj} - 2\xi \dot{\gamma}_{kl} \frac{\partial a_{mnkl}}{\partial a_{ij}} \quad 22$$

$$\frac{\partial \dot{a}_{mn}^{IRD}}{\partial a_{ij}} = -2D_r\alpha\delta_{mi}\delta_{nj} \quad 23$$

The same equation of change can be developed for the 4th order tensor in terms of the 4th and 6th order tensor and subsequently for even higher orders hence to obtain a closed set of equations, closure approximation is required. Different closures approximation for the 4th order tensor and their derivatives have been investigated and discussed in later sections.

Since there are only 5 independent components of the 2nd order tensor a_{ij} , in contracted notation, we can represent the residual R_{mn}^{FT} as a vector R_r^{FT} and the Jacobian J_{mnij}^{FT} as a matrix J_{rs}^{FT} . Any reordering convention could be used. Here we employ.

$$r(m,n) = n - \frac{1}{2}(m-1)(m-6), \quad \text{for } n = m \dots 3, \quad \text{for } m = 1, 2 \quad 24$$

2. Strain Reduction Factor (SRF) Model

The SRF model was developed by Huynh [8] as an improvement to the FT model where he applied a strain reduction factor $\frac{1}{\kappa}$ directly to the to the FT model to slow down the orientation kinetics as observed experimentally. He based his premise on a reduced bulk strain of fiber clusters in a concentrated suspension flow. Although the predictions of the steady state orientation based on this model for simple shear flow with suitable determination of κ matched experimental results [9], however it gave an initial overshoot at small strain. The residual and Jacobian in this case is just a multiplication of κ with that previously obtained for the FT model.

$$R_{mn}^{SRF} = \kappa R_{mn}^{FT}, \quad J_{mnij}^{FT} = \kappa J_{mnij}^{FT}, \quad 0 < \kappa < 1 \quad 25$$

The SRF model does not satisfy the rheological test of material non-objectivity and results are dependent on the coordinate system and cannot be applied to complex flows.

3. Reduced Strain Closure (RSC) Model

To address the material non-objectivity drawback of the SRF model, Wang et al [9] developed a reduced strain closure (RSC) model where he applied the reduction factor only to the evolution rate of the spectral decomposed principal directions of the orientation tensor $\underline{\lambda}$, without modifying the rate of the rotation $\underline{\dot{\phi}}$ i.e.

$$\dot{\lambda}_i^{RSC} = \kappa \dot{\lambda}_i^{FT}, \quad \dot{\phi}_{ij}^{RSC} = \dot{\phi}_{ij}^{FT}, \quad a_{mn}|a_{mn} = \lambda_i \phi_{mi} \phi_{ni} \quad 26$$

Based on this model, the modified material derivative is thus [9]

$$\begin{aligned} \dot{a}_{mn}^{RSC} &= \dot{a}_{mn}^{FT} - (1 - \kappa) \dot{a}_{mn}^{\Delta FT} \\ \dot{a}_{mn}^{\Delta FT} &= 2\xi \dot{\gamma}_{kl} (L_{mnkl} - M_{mnrs} a_{rskl}) + \dot{a}_{mn}^{IRD} \end{aligned} \quad 27$$

where,

$$L_{mnkl} = \dot{\lambda}_i \phi_{mi} \phi_{ni} \phi_{ki} \phi_{li}, \quad M_{mnkl} = \phi_{mi} \phi_{ni} \phi_{ki} \phi_{li} \quad 28$$

The Newton Raphson residual is thus $R_{mn}^{RSC} = \dot{a}_{mn}^{RSC}$ and the Jacobian is obtained by taking partial derivatives thus

$$J_{mnij}^{RSC} = J_{mnij}^{FT} - (1 - \kappa) \frac{\partial \dot{a}_{mn}^{\Delta FT}}{\partial a_{ij}} \quad 29$$

where,

$$\frac{\partial \dot{a}_{mn}^{\Delta FT}}{\partial a_{ij}} = 2\xi \dot{\gamma}_{kl} \frac{\partial}{\partial a_{ij}} \{L_{mnkl} - M_{mnrs} a_{rskl}\} + \frac{\partial \dot{a}_{mn}^{IRD}}{\partial a_{ij}} \quad 30$$

expanding eqn. 30 above based on the distributive properties of differentiation we obtain

$$\frac{\partial \dot{a}_{mn}^{\Delta FT}}{\partial a_{ij}} = \xi \dot{\gamma}_{kl} \left[\frac{\partial L_{mnkl}}{\partial a_{ij}} - a_{rskl} \frac{\partial M_{mnrs}}{\partial a_{ij}} - M_{mnrs} \frac{\partial a_{rskl}}{\partial a_{ij}} \right] + \frac{\partial \dot{a}_{mn}^{IRD}}{\partial a_{ij}} \quad 31$$

Applying the product rule of differentiation, we obtain the derivatives of 4th order tensors M_{mnkl} and L_{mnkl} respectively.

$$\begin{aligned} \frac{\partial M_{mnkl}}{\partial a_{rs}} &= \frac{\partial}{\partial a_{rs}} \{ \phi_{mi} \phi_{ni} \phi_{ki} \phi_{li} \} \\ &= \phi_{ni} \phi_{ki} \phi_{li} \frac{\partial \phi_{mi}}{\partial a_{rs}} + \phi_{mi} \phi_{ki} \phi_{li} \frac{\partial \phi_{ni}}{\partial a_{rs}} + \phi_{mi} \phi_{ni} \phi_{li} \frac{\partial \phi_{ki}}{\partial a_{rs}} \\ &\quad + \phi_{mi} \phi_{ni} \phi_{ki} \frac{\partial \phi_{li}}{\partial a_{rs}} \end{aligned} \quad 32$$

and

$$\frac{\partial L_{mnkl}}{\partial a_{rs}} = \Phi_{mi} \Phi_{ni} \Phi_{ki} \Phi_{li} \frac{\partial \dot{\lambda}_i}{\partial a_{rs}} + \dot{\lambda}_i \frac{\partial}{\partial a_{rs}} \{ \Phi_{mi} \Phi_{ni} \Phi_{ki} \Phi_{li} \} \quad 33$$

Where the procedure for obtaining the derivatives of the eigenvalues and eigenvectors kindly can be found in Appendix I.

4. Retarding Principal Rate (RPR) Model

Tseng et al [10] likewise developed a retarding principal rate (*RPR*) model like the RSC model, to slow down the fiber orientation kinetics based on a coaxial modification to the principal directions of the orientation tensor evolution rate via a nonlinear correlation. The material derivative tensor of any standard model \dot{a}_{mn}^X can be linearly superposed to its RPR correction to slow down the response rate. i.e.

$$\dot{a}_{mn}^{X-RPR} = \dot{a}_{mn}^X + \dot{a}_{mn}^{RPR} \quad 34$$

where the RPR correction \dot{a}_{mn}^{RPR} is given as

$$\dot{a}_{mn}^{RPR} = -\Phi_{mk} \dot{\Lambda}_{kl}^{IOK} \Phi_{nl}, \quad \dot{\Lambda}_{kl}^{IOK} = \dot{\Lambda}_{kl}^{IOK}(\underline{\dot{\lambda}}^X) \quad 35$$

Because the correction is coaxial, the rotation tensor growth rate is unaffected and is obtained from the spectral decomposition of a_{mn}^X . i.e.,

$$\underline{\underline{\Phi}} \mid \Lambda_{mn}^X = \Phi_{km} a_{kl}^X \Phi_{ln} \quad 36$$

The columns of the eigenmatrix obtained in this way are reordered in descending order with the magnitude of the eigenvalues i.e.,

$$\Phi_{ij} = \{ \Phi_{ij} \mid \lambda_j^X = \Lambda_{jj}^X, \quad \lambda_1^X \geq \lambda_2^X \geq \lambda_3^X \} \quad 37$$

The growth rate of the principal eigenvalues of the standard model $\dot{\Lambda}_{kl}^X$ is obtained from

$$\dot{\Lambda}_{kl}^X = \Phi_{km} \dot{a}_{kl}^X \Phi_{ln}, \quad \dot{\lambda}_k^X = \dot{\Lambda}_{kk}^X \quad 38$$

The correction to the principal values of the material derivative of the orientation tensor based on the IOK assumption $\dot{\Lambda}_{kk}^{IOK}$ is defined by a 2-parameter non-linear correlation to the principal values of the standard model $\dot{\Lambda}_{kl}^X$ such that.

$$\dot{\Lambda}_{kk}^{IOK} = \dot{\lambda}_k^{IOK} = \alpha \left[\dot{\lambda}_k^X - \beta \left(\{ \dot{\lambda}_k^X \}^2 + 2 \dot{\lambda}_l^X \dot{\lambda}_m^X \right) \right], \quad \dot{\Lambda}_{kl}^{IOK} \Big|_{k \neq l} = 0 \quad 39$$

For an RPR corrected model, the NT residual R_{mn}^{X-RPR} is simply the material derivative, i.e.,

$$R_{mn}^{X-RPR} = \dot{a}_{mn}^{X-RPR} \quad 40$$

and Jacobian J_{mni}^{X-RPR} is given as

$$J_{mni}^{X-RPR} = \frac{\partial \dot{a}_{mn}^X}{\partial a_{ij}} + \frac{\partial \dot{a}_{mn}^{RPR}}{\partial a_{ij}} \quad 41$$

The partial derivative of the RPR correction term \dot{a}_{mn}^{RPR} is given as

$$\frac{\partial \dot{a}_{mn}^{RPR}}{\partial a_{ij}} = - \left\{ \frac{\partial \Phi_{mk}}{\partial a_{ij}} \dot{\Lambda}_{kl}^{IOK} \Phi_{nl} + \Phi_{mk} \frac{\partial \dot{\Lambda}_{kl}^{IOK}}{\partial a_{ij}} \Phi_{nl} + \Phi_{mk} \dot{\Lambda}_{kl}^{IOK} \frac{\partial \Phi_{nl}}{\partial a_{ij}} \right\} \quad 42$$

And the partial derivative of the modified growth rate of eigenvalues tensor $\dot{\Lambda}_{kl}^{IOK}$ is given as

$$\frac{\partial \dot{\Lambda}_{kk}^{IOK}}{\partial a_{ij}} = \frac{\partial \dot{\lambda}_k^{IOK}}{\partial a_{ij}} = \alpha \left[\frac{\partial \dot{\lambda}_k^X}{\partial a_{ij}} - 2\beta \left(\dot{\lambda}_k^X \frac{\partial \dot{\lambda}_k^X}{\partial a_{ij}} + \frac{\partial \dot{\lambda}_i^X}{\partial a_{ij}} \dot{\lambda}_m^X + \dot{\lambda}_i^X \frac{\partial \dot{\lambda}_m^X}{\partial a_{ij}} \right) \right], \quad \left. \frac{\partial \dot{\Lambda}_{kl}^{IOK}}{\partial a_{ij}} \right|_{k \neq l} = 0 \quad 43$$

where

$$\frac{\partial \dot{\Lambda}_{kl}^X}{\partial a_{ij}} = \left\{ \frac{\partial \Phi_{km}}{\partial a_{ij}} \dot{a}_{kl}^X \Phi_{ln} + \Phi_{km} \frac{\partial \dot{a}_{kl}^X}{\partial a_{ij}} \Phi_{ln} + \Phi_{km} \dot{a}_{kl}^X \frac{\partial \Phi_{ln}}{\partial a_{ij}} \right\}, \quad \frac{\partial \dot{\lambda}_k^X}{\partial a_{ij}} = \frac{\partial \dot{\Lambda}_{kk}^X}{\partial a_{ij}} \quad 44$$

$\frac{\partial \dot{a}_{mn}^X}{\partial a_{ij}}$ is the partial derivative material derivative of the 2nd order orientation tensor with respect to its components obtained a priori and the partial derivatives of the eigenmatrix with respect to the same (i. e., $\frac{\partial \Phi_{mn}}{\partial a_{ij}}$) can be obtained through any method in Appendix I

5. Anisotropic Rotary Diffusion (ARD) Models

While the IRD models were experimental observed to be accurate in predicting the orientation state of short-fiber/thermoplastic composites (SFT) they were ineffective in accurately predicting the complete set of orientation tensor components for the long-fiber/thermoplastic composites (LFT) which was the motivation for ARD model development. Various ARD models with different modifications have been developed based on the definition of the spatial diffusion tensor. Most models utilize the moment-tensor form for the ARD representation developed by Phelps and Tucker [12]. The general expression for the 2nd order orientation tensor evolution rate is a linear combination of the Jeffery's model and the and the rotary diffusion term given as

$$\dot{a}_{mn}^{PT} = \dot{a}_{mn}^{HD} + \dot{a}_{mn}^{ARD} \quad 45$$

where the rotary diffusion term \dot{a}_{mn}^{ARD} is defined in terms of the spatial diffusion coefficient and the orientation state and is given as

$$\dot{a}_{mn}^{ARD} = \dot{\gamma} [2C_{mn} - 2C_{rs}\delta_{rs}a_{mn} - 5(C_{mk}a_{kn} + a_{mk}C_{kn}) + 10a_{mnkl}C_{kl}] \quad 46$$

and \underline{C} is the spatial diffusion tensor. Based on this model, the NT residual and Jacobian are respectively given as

$$R_{mn}^{PT} = \dot{a}_{mn}^{PT} \quad 47$$

$$J_{mnij}^{PT} = \frac{\partial \dot{a}_{mn}^{PT}}{\partial a_{ij}} = \frac{\partial \dot{a}_{mn}^{HD}}{\partial a_{ij}} + \frac{\partial \dot{a}_{mn}^{ARD}}{\partial a_{ij}} \quad 48$$

Where the derivative of the rotary diffusion (ARD) term is obtained using product rule as

$$\begin{aligned} \frac{\partial \dot{a}_{mn}^{ARD}}{\partial a_{ij}} = \dot{\gamma} & \left[2 \frac{\partial C_{mn}}{\partial a_{ij}} - 2 \left(\frac{\partial C_{rs}}{\partial a_{ij}} \delta_{rs} a_{mn} + C_{rs} \delta_{rs} \delta_{mi} \delta_{nj} \right) + \dots \right. \\ & - 5 \left(\frac{\partial C_{mk}}{\partial a_{ij}} a_{kn} + C_{mk} \delta_{ki} \delta_{nj} + \delta_{mi} \delta_{kj} C_{kn} + a_{mk} \frac{\partial C_{kn}}{\partial a_{ij}} \right) + \dots \\ & \left. + 10 \left(\frac{\partial a_{mnkl}}{\partial a_{ij}} C_{kl} + a_{mnkl} \frac{\partial C_{kl}}{\partial a_{ij}} \right) \right] \quad 49 \end{aligned}$$

In the mold-flow ARD (*mARD*) model developed by Bakharev A [20], the Phelps & Tucker's rotary diffusion (*ARD*) expression is truncated to include just the linear terms. i.e.

$$\dot{a}_{mn}^{mARD} = \dot{\gamma}[2C_{mn} - 2C_{kl}\delta_{kl}a_{mn}] \quad 50$$

$$\frac{\partial \dot{a}_{mn}^{mARD}}{\partial a_{ij}} = \dot{\gamma} \left[2 \frac{\partial C_{mn}}{\partial a_{ij}} - 2 \left(\frac{\partial C_{kl}}{\partial a_{ij}} \delta_{kl} a_{mn} + C_{kl} \delta_{kl} \delta_{mi} \delta_{nj} \right) \right] \quad 51$$

The corresponding evolution rate equation for the 2nd order orientation tensor based on *mARD* model is given as

$$\dot{a}_{mn}^{mPT} = \dot{a}_{mn}^{HD} + \dot{a}_{mn}^{mARD} \quad 52$$

Various models for the spatial diffusion coefficient C_{mn} used in the ARD model have been developed by various researchers. The basic representation of C_{mn} by Phelps and Tucker [12] based on a modification of Hand's anisotropic tensor [17] is given as a function of the rate of deformation tensor and orientation state as

$$C_{mn}^{PT} = b_1 \delta_{mn} + b_2 a_{mn} + b_3 a_{mk} a_{nk} + \frac{b_4}{\dot{\gamma}} \dot{\gamma}_{mn} + \frac{b_5}{\dot{\gamma}^2} \dot{\gamma}_{mk} \dot{\gamma}_{nk} \quad 53$$

Where b_i are dimensionless constants obtained from regression analysis of experimental data. For this model, the derivative of the C_{mn}^{PT} with respect to a_{ij} is given as

$$\frac{\partial C_{mn}^{PT}}{\partial a_{ij}} = b_2 \delta_{mi} \delta_{nj} + b_3 (\delta_{mi} \delta_{kj} a_{nk} + a_{mk} \delta_{ni} \delta_{kj}) \quad 54$$

The sensitivity of the PT model parameters b_i to ensure numerical stability of the model response coupled with the complicated process involved in their determination were the major limitations to this model application. Tseng et al [18] developed an improved anisotropic rotary diffusion model (*iARD*) based on a definition of a two-parameter spatial diffusion tensor model in terms of the rate of deformation tensor that couples the effect of fiber-matrix interaction and fiber-fiber interaction given as

$$C_{mn}^{iARD} = C_I \left(\delta_{mn} - 4C_M \frac{\dot{\gamma}_{mk} \dot{\gamma}_{nk}}{\dot{\gamma}^2} \right) \quad 55$$

Where C_I & C_M are the fiber-fiber and fiber-matrix interaction parameters respectively. An alternate definition is given as

$$C_{mn}^{iARD} = C_I (\delta_{mn} - C_M \tilde{L}_{mn}), \quad \tilde{L}_{mn} = (L_{mk} L_{nk}) / (L_{rs} L_{rs}) \quad 56$$

The derivative of the spatial diffusion tensor with respect to the 2nd order orientation tensor is simply zero. i.e.,

$$\frac{\partial C_{mn}^{iARD}}{\partial a_{ij}} = 0 \quad 57$$

Because of the material non-objectivity of the rate of deformation tensor L_{mn} used in the definition of the spatial diffusion tensor C_{mn} in the *iARD* model, Tseng et. al [19] developed an improved objective principal spatial tensor ARD model (*pARD*) that is coaxial with the orientation tensor given as

$$C_{mn}^{pARD} = \left\{ C_I \Phi_{mk} D_{kl} \Phi_{nl}, \quad \underline{\Phi} | a_{mn} = \Phi_{mk} \bar{a}_{kl} \Phi_{nl} \right\} \quad 58$$

Where the tensor D_{kl} contains only diagonal terms and its trace is unity. i.e.

$$D_{kl} \delta_{kl} = D_{kk} = 1, \quad D_{kl} |_{k \neq l} = 0 \quad 59$$

The derivative of C_{mn}^{pARD} with respect to the 2nd order orientation tensor is given as

$$\frac{\partial C_{mn}^{pARD}}{\partial a_{ij}} = C_I \left\{ \frac{\partial \Phi_{mk}}{\partial a_{ij}} D_{kl} \Phi_{nl} + \Phi_{mk} D_{kl} \frac{\partial \Phi_{nl}}{\partial a_{ij}} \right\} \quad 60$$

Another ARD model reduction suggested by Wang [51] called the WPT model involved truncating the terms of the PT model to just the first and third term such that,

$$C_{mn}^{WPT} = b_1 \delta_{mn} + b_3 a_{mk} a_{nk} \quad 61$$

Falvoro et al [23] provided an alternative form of the spatial diffusion tensor where he replaced the coefficients with a weighted superposition of the interaction coefficient, i.e.

$$C_{mn}^{WPT} = C_I ((1 - w) \delta_{mn} + w a_{mk} a_{nk}) \quad 62$$

Where w is the weighting factor. The derivative of C_{mn}^{pARD} with respect to the 2nd order orientation tensor is given as

$$\frac{\partial C_{mn}^{WPT}}{\partial a_{ij}} = w C_I (\delta_{mk} a_{nk} + a_{mk} \delta_{nk}) \quad 63$$

Lastly, we consider the D_z ARD model development (cf. Falvoro et. al [23]) by Moldflow for simulating 2.5D flow processes. Their model is defined in terms of the interaction coefficient, C_I , a moment of interaction thickness parameter D_z , and the unit normal to the mold surface \hat{n} . The expression for C_{mn} here is given as

$$C_{mn}^{Dz} = C_I^{Dz} (\delta_{mn} - (1 - D_z) \hat{n}_m \hat{n}_n) \quad 64$$

And

$$\frac{\partial C_{mn}^{Dz}}{\partial a_{ij}} = 0 \quad 65$$

6. Nematic Potential (NEM) Model

Latz et al [21] proposed a 2-parameter nematic potential ARD (*NEM*) model for the diffusion term that couples the phenomenological effect of the momentum diffusion due to fiber-fiber interaction and a topological interaction effect of diffusion due to an exclusion volume mechanism. i.e.

$$\dot{a}_{mn}^{IRD-MS} = \dot{\gamma} [C_I (\delta_{mn} - \alpha a_{mn}) + U_0 (a_{mk} a_{kn} - a_{kl} a_{mnkl})] \quad 66$$

where U_0 is the ‘Onsager’ nematic topological interaction coefficient of the Maier-Saupe potential. Typically, for stability, $U_0 \leq 4C_I$ for 2D analysis and $U_0 > 8C_I$ for 3D analysis. The material derivative of the 2nd order orientation tensor based on the nematic diffusion model is thus given as

$$\dot{a}_{mn}^{nem} = \dot{a}_{mn}^{HD} + \dot{a}_{mn}^{IRD-MS} \quad 67$$

The NT residual and Jacobian are respectively given as

$$R_{mn}^{nem} = \dot{a}_{mn}^{nem} \quad 68$$

$$J_{mni}^{nem} = \frac{\partial \dot{a}_{mn}^{HD}}{\partial a_{ij}} + \frac{\partial \dot{a}_{mn}^{IRD-MS}}{\partial a_{ij}} \quad 69$$

Where the derivative of the nematic diffusion term is given as

$$\frac{\partial \dot{a}_{mn}^{IRD-MS}}{\partial a_{ij}} = \dot{\gamma} \left[-C_I \alpha \delta_{mi} \delta_{nj} + U_0 \left(\delta_{mi} \delta_{kj} a_{kn} + a_{mk} \delta_{ki} \delta_{nj} - \delta_{ki} \delta_{lj} a_{mnkl} - a_{kl} \frac{\partial a_{mnkl}}{\partial a_{ij}} \right) \right] \quad 70$$

Most commercial software used in simulation of the injection molding process such as Autodesk Moldflow, Moldex3D usually combines multiple models in predicting the orientation state for improved accuracy. One such combination is the ARD-RSC models whose material derivative is expressed as

$$\dot{a}_{mn}^{pARD-RSC} = \dot{a}_{mn}^{RSC} - \kappa \dot{a}_{mn}^{IRD} + \dot{a}_{mn}^{ARD} + \dot{a}_{mn}^{\Delta RSC} \quad 71$$

where,

$$\dot{a}_{mn}^{\Delta RSC} = -2\dot{\gamma}(1 - \kappa)[M_{mnkl} - \delta_{kl}a_{mn} - 5(L_{mnkl} - M_{mnrs}a_{rskl})]C_{kl} \quad 72$$

and \dot{a}_{mn}^{RSC} , \dot{a}_{mn}^{IRD} , \dot{a}_{mn}^{ARD} have been defined in preceding sections. In this case the NT residual $R_{mn}^{pARD-RSC}$ is the material derivative $\dot{a}_{mn}^{pARD-RSC}$, i.e.,

$$R_{mn}^{pARD-RSC} = \dot{a}_{mn}^{pARD-RSC} \quad 73$$

And the Jacobian is obtained by taking partial derivatives with respect to the 2nd order tensor as usual and can be expressed as

$$J_{mij}^{pARD-RSC} = \frac{\partial \dot{a}_{mn}^{RSC}}{\partial a_{ij}} - \kappa \frac{\partial \dot{a}_{mn}^{IRD}}{\partial a_{ij}} + \frac{\partial \dot{a}_{mn}^{ARD}}{\partial a_{ij}} + \frac{\partial \dot{a}_{mn}^{\Delta RSC}}{\partial a_{ij}} \quad 74$$

where

$$\frac{\partial \dot{a}_{mn}^{\Delta RSC}}{\partial a_{ij}} = -2\dot{\gamma}(1 - \kappa) \left\{ \begin{array}{l} \left[\frac{\partial M_{mnkl}}{\partial a_{ij}} - \delta_{kl}\delta_{mi}\delta_{nj} - 5 \frac{\partial}{\partial a_{ij}} \{L_{mnkl} - M_{mnrs}a_{rskl}\} \right] C_{kl} + \dots \\ [M_{mnkl} - \delta_{kl}a_{mn} - 5(L_{mnkl} - M_{mnrs}a_{rskl})] \frac{\partial C_{kl}}{\partial a_{ij}} \end{array} \right\} \quad 75$$

All terms of the partial derivatives have been previously derived in preceding section.

Closure Approximations and Their Explicit Derivatives

Derivatives of the orientation tensor closure approximation are used in the Newton-Raphson iteration method to compute the steady-state fiber orientation tensor state. These derivatives for the various closure approximation used in this study appear below.

(a) Quadratic Closure Approximation – \tilde{a}_4

The quadratic closure was introduced by Doi [33] and Lipscomb [34] and defined as dyadic product of the 2nd order orientation tensor. We denote the quadratic closure approximate \tilde{a}_4 and is mathematically given as

$$\tilde{a}_4 = \tilde{a}_{ijkl} = a_2 a_2 = a_{ij} a_{kl} \quad 76$$

The derivative of \tilde{a}_4 above with respect to the 2nd order tensor a_{mn} is simply.

$$\frac{\partial \tilde{a}_{ijkl}}{\partial a_{mn}} = \frac{\partial a_{ij}}{\partial a_{mn}} a_{kl} + a_{ij} \frac{\partial a_{kl}}{\partial a_{mn}} = \delta_{im}\delta_{jn}a_{kl} + a_{ij}\delta_{km}\delta_{ln} \quad 77$$

(b) Linear Closure Approximation – \hat{a}_4

The linear closure approximation of \hat{a}_4 first proposed by Hand [17] using all the products of a_2 and δ is given as

$$\hat{a}_4 = \hat{a}_{ijkl} = -h_1(\delta_{ij}\delta_{kl} + \delta_{ik}\delta_{jl} + \delta_{il}\delta_{jk}) + h_2(a_{ij}\delta_{kl} + a_{ik}\delta_{jl} + a_{il}\delta_{jk} + \delta_{ij}a_{kl} + \delta_{ik}a_{jl} + \delta_{il}a_{jk}) \quad 78$$

The derivative of \hat{a}_4 above with respect to components of the 2nd order tensor a_{mn} is given as

$$\frac{\partial \hat{a}_{ijkl}}{\partial a_{mn}} = h_2(\delta_{im}\delta_{jn}\delta_{kl} + \delta_{im}\delta_{kn}\delta_{jl} + \delta_{im}\delta_{ln}\delta_{jk} + \delta_{im}\delta_{jn}\delta_{kl} + \delta_{im}\delta_{kn}\delta_{jl} + \delta_{im}\delta_{ln}\delta_{jk}) \quad 79$$

where h_1 and h_2 are numerical factors which varies based on spatial dimensionality as

	<i>3D – Space</i>	<i>2D – Planar</i>
h_1	$\frac{1}{35}$	$\frac{1}{24}$
h_2	$\frac{1}{7}$	$\frac{1}{6}$

(c) Hybrid Closure Approximation – a_4

The hybrid closure approximation a_4 is simply combination of both linear \hat{a}_{ijkl} and quadratic \tilde{a}_{ijkl} closure approximation above by some scalar measure of orientation f given as [7]

$$a_4 = a_{ijkl} = f\tilde{a}_{ijkl} + (1 - f)\hat{a}_{ijkl} \quad 80$$

Where f is a generalization of Herman's Orientation factor. Advani & Tucker [7] proposed an appropriate approximation of as $f = a_f a_{ij} a_{ji} - b_f$, where a_f and b_f are constants that depends on the given dimension thus

	<i>3D – Space</i>	<i>2D – Planar</i>
a_f	$\frac{3}{2}$	2
b_f	$\frac{1}{2}$	1

the derivative of the hybrid closure approximation a_4 with respect to components of the 2nd order tensor a_{mn} is given as

$$\frac{\partial a_{ijkl}}{\partial a_{mn}} = f \frac{\partial \tilde{a}_{ijkl}}{\partial a_{mn}} + (1 - f) \frac{\partial \hat{a}_{ijkl}}{\partial a_{mn}} + \frac{\partial f}{\partial a_{mn}} (\tilde{a}_{ijkl} - \hat{a}_{ijkl}) \quad 81$$

where,

$$\frac{\partial f}{\partial a_{mn}} = a_f (\delta_{im}\delta_{jn}a_{ji} + a_{ij}\delta_{jm}\delta_{in}) \quad 82$$

An alternative estimation of the factor f by Advani & Tucker [7] is given as

$$f = 1 - \alpha^\alpha e_{ijk} a_{i1} a_{j2} a_{k3} \quad 83$$

$$\frac{\partial f}{\partial a_{mn}} = -\alpha^\alpha e_{ijk} \{ \delta_{im}\delta_{1n}a_{j2}a_{k3} + a_{i1}\delta_{jm}\delta_{2n}a_{k3} + a_{i1}a_{j2}\delta_{km}\delta_{3n} \} \quad 84$$

(d) Hinch and Leal Closure Approximation

The Hinch and Leal closure approximations were not explicit expressions of the 4th order orientation tensor a_{ijkl} but were in contracted form with the deformation rate tensor i.e., $\gamma_{kl}a_{ijkl}$. Advani and Tucker developed a general explicit expression of a_{ijkl} (eqn. 85) summarizing all the Hinch and Leal closures forms.

$$a_{ijkl} = \beta_1(\delta_{ij}\delta_{kl}) + \beta_2(\delta_{ik}\delta_{jl} + \delta_{il}\delta_{jk}) + \beta_3(\delta_{ij}a_{kl} + a_{ij}\delta_{kl}) \\ + \beta_4(a_{ik}\delta_{jl} + a_{jl}\delta_{ik} + a_{il}\delta_{jk} + a_{jk}\delta_{il}) + \beta_5(a_{ij}a_{kl}) + \beta_6(a_{ik}a_{jl} + a_{il}a_{jk}) \\ + \beta_7(\delta_{ij}a_{km}a_{ml} + a_{im}a_{mj}\delta_{kl}) + \beta_8(a_{im}a_{mj}a_{kn}a_{nl}) \quad 85$$

And the partial derivative of the above expression with respect to components of the 2nd order orientation tensor a_{rs} based on product rule is given as

$$\frac{\partial a_{ijkl}}{\partial a_{rs}} = \left[\frac{\partial \beta_1}{\partial a_{rs}}(\delta_{ij}\delta_{kl}) + \frac{\partial \beta_2}{\partial a_{rs}}(\delta_{ik}\delta_{jl} + \delta_{il}\delta_{jk}) + \frac{\partial \beta_3}{\partial a_{rs}}(\delta_{ij}a_{kl} + a_{ij}\delta_{kl}) \right. \\ + \frac{\partial \beta_4}{\partial a_{rs}}(a_{ik}\delta_{jl} + a_{jl}\delta_{ik} + a_{il}\delta_{jk} + a_{jk}\delta_{il}) + \frac{\partial \beta_5}{\partial a_{rs}}(a_{ij}a_{kl}) + \frac{\partial \beta_6}{\partial a_{rs}}(a_{ik}a_{jl} + a_{il}a_{jk}) \\ + \frac{\partial \beta_7}{\partial a_{rs}}(\delta_{ij}a_{km}a_{ml} + a_{im}a_{mj}\delta_{kl}) + \left. \frac{\partial \beta_8}{\partial a_{rs}}(a_{im}a_{mj}a_{kn}a_{nl}) \right] + \dots \quad 86 \\ + \left[\beta_3(\delta_{ij}\delta_{kr}\delta_{ls} + \delta_{ir}\delta_{js}\delta_{kl}) + \beta_4(\delta_{ir}\delta_{ks}\delta_{jl} + \delta_{jr}\delta_{ls}\delta_{ik} + \delta_{ir}\delta_{ls}\delta_{jk} + \delta_{jr}\delta_{ks}\delta_{il}) \right. \\ + \beta_5(\delta_{ir}\delta_{js}a_{kl} + a_{ij}\delta_{kr}\delta_{ls}) + \beta_6(\delta_{ir}\delta_{ks}a_{jl} + a_{ik}\delta_{jr}\delta_{ls} + \delta_{ir}\delta_{ls}a_{jk} + a_{il}\delta_{jr}\delta_{ks}) \\ + \beta_7(\delta_{ij}\delta_{kr}\delta_{ms}a_{ml} + \delta_{ij}a_{km}\delta_{mr}\delta_{ls} + \delta_{ir}\delta_{ms}a_{mj}\delta_{kl} + a_{im}\delta_{mr}\delta_{js}\delta_{kl}) \\ \left. + \beta_8(\delta_{ir}\delta_{ms}a_{mj}a_{kn}a_{nl} + a_{im}\delta_{mr}\delta_{js}a_{kn}a_{nl} + a_{im}a_{mj}\delta_{kr}\delta_{ns}a_{nl} + a_{im}a_{mj}a_{kn}\delta_{nr}\delta_{ls}) \right]$$

Mullens [42] provided a summary Table (cf. Table 1) for the β_i factors of the Hinch and Leal closures subdivided into weak flow (WF - Isotropic, Linear and Quadratic), strong flow (SF), and Hinch and Leal composite flows (HL - HL1&HL2) closure forms.

		β_1	β_2	β_3	β_4	β_5	β_6	β_7	β_8
WF	ISO	$\frac{1}{15}$	$\frac{1}{15}$
	LIN	$-\frac{1}{35}$	$-\frac{1}{35}$	$\frac{1}{7}$	$\frac{1}{7}$
	QDR	1
SF	SF2	1	1	...	$-\frac{2}{\langle a^2 \rangle}$
HL	HL1	$\frac{2}{5}$...	$-\frac{1}{5}$	$\frac{3}{5}$	$-\frac{2}{5}$...
	HL2	$\frac{26}{315}\alpha$	$\frac{26}{315}\alpha$	$\frac{16}{63}\alpha$	$-\frac{4}{21}\alpha$	1	1	...	$-\frac{2}{\langle a^2 \rangle}$

Table 1: Summary of the Hinch and Leal closure β_i factors for the different flow classifications

Where the parameters $\langle a^2 \rangle$ and α are respectively

$$\langle a^2 \rangle = a_{ij}a_{ji}, \quad \alpha = \exp \left[2 \frac{1 - 3\langle a^2 \rangle}{1 - \langle a^2 \rangle} \right] \quad 87$$

And the partial derivatives are respectively given as

$$\frac{\partial \langle a^2 \rangle}{\partial a_{rs}} = \delta_{ir}\delta_{js}a_{ji} + a_{ij}\delta_{jr}\delta_{is}, \quad \frac{\partial \alpha}{\partial a_{rs}} = -\frac{4\alpha}{(1 - \langle a^2 \rangle)^2} \frac{\partial \langle a^2 \rangle}{\partial a_{rs}}, \quad \frac{\partial}{\partial a_{rs}} \left\{ \frac{k}{\langle a^2 \rangle} \right\} = -\frac{k}{\langle a^2 \rangle^2} \frac{\partial \langle a^2 \rangle}{\partial a_{rs}} \quad 88$$

(e) Eigenvalue based Orthotropic Fitted (EBF) Closure Approximations

The idea of orthotropic closure approximations for the 4th order tensor was to impose objectivity such that the approximation is independent of the coordinate frame selection. In essence, the principal axes of the closure approximation and second order tensor must coincide. The (9x9) term 4th order tensor can be represented in (6 x 6) contracted notation like in structural analysis of composite material based on symmetry property. i.e.

$$A_{rs} = a_{ijkl} \quad 89$$

Where, the index of the contracted notation is related to the index notation according to

$$r = \begin{cases} i = j & \delta_{ij} = 1 \\ (9 - i - j) & \delta_{ij} = 0 \end{cases} \quad \& \quad s = \begin{cases} k = l & \delta_{kl} = 1 \\ (9 - k - l) & \delta_{kl} = 0 \end{cases} \quad 90$$

The derivative of the 4th order tensor with respect to the 2nd order tensor is such that

$$\frac{\partial A_{rs}}{\partial a_{mn}} = \frac{\partial a_{ijkl}}{\partial a_{mn}} \quad 91$$

Symmetry property of the 4th order tensor requires $a_{ijkl} = a_{klij}$ which implies that $A_{rs} = A_{sr}$. The contracted tensor A_{rs} transformed to the principal axes has the orthotropic form \bar{A}_{rs} given thus.

$$\underline{\bar{A}} = \begin{bmatrix} \bar{A}_{11} & \bar{A}_{12} & \bar{A}_{13} & & & \\ \bar{A}_{21} & \bar{A}_{22} & \bar{A}_{23} & & & \\ \bar{A}_{31} & \bar{A}_{32} & \bar{A}_{33} & & & \\ & & & \bar{A}_{44} & & \\ & & & & \bar{A}_{55} & \\ & & & & & \bar{A}_{66} \end{bmatrix} \quad 92$$

The contracted tensor transforms from its principal reference frame to the original coordinate axes according to

$$\underline{\bar{A}} = \underline{\underline{M}}^T \underline{\bar{A}} \underline{\underline{M}}, \quad \text{or,} \quad A_{rs} = M_{ri}M_{sj}\bar{A}_{ij} \quad 93$$

The 6x6 transformation matrix $\underline{\underline{M}}$ is given as $\underline{\underline{M}} = \underline{\underline{F}} \underline{\underline{Q}} \underline{\underline{F}}^{-1}$, where $F_{ij} = k\delta_{ij}$, $k = \begin{cases} 1 & i \leq 3 \\ 2 & i > 3 \end{cases}$ and

$Q_{rs} = q_{ik}q_{jl} + (1 - \delta_{kl})q_{jk}q_{il}$. The modal matrix $\underline{\underline{q}}$ whose kth column are the corresponding eigenvectors $\underline{\underline{x}}^k$ of eigenvalues \bar{a}_k is obtained from the spectral decomposition of $\underline{\underline{a}}$ is such that:

$$\underline{\underline{\bar{a}}} = \begin{bmatrix} \lambda_1 & & \\ & \lambda_2 & \\ & & \lambda_3 \end{bmatrix} = \underline{\underline{q}}^T \underline{\underline{a}} \underline{\underline{q}} \quad 94$$

The indices of the contracted 4th order modal tensor Q_{rs} relates to the those of the 2nd order modal matrix $\underline{\underline{q}}$ according to above equation. A more direct way is to reconstruct the 4th order orientation tensor $\underline{\underline{\bar{a}}}_{mnpq}$ from the contracted form A_{rs} and transform from the principal reference frame to the original axes according to eqn. 95 below.

$$a_{ijkl} = q_{im}q_{jn}q_{kp}q_{lq}\bar{a}_{mnpq} \quad 95$$

And using the product rule

$$\begin{aligned} \frac{\partial a_{ijkl}}{\partial a_{rs}} &= q_{im}q_{jn}q_{kp}q_{lq} \frac{\partial \bar{a}_{mnpq}}{\partial a_{rs}} + \dots \\ &+ \left(\frac{\partial q_{im}}{\partial a_{rs}} q_{jn}q_{kp}q_{lq} + q_{im} \frac{\partial q_{jn}}{\partial a_{rs}} q_{kp}q_{lq} + q_{im}q_{jn} \frac{\partial q_{kp}}{\partial a_{rs}} q_{lq} + q_{im}q_{jn}q_{kp} \frac{\partial q_{lq}}{\partial a_{rs}} \right) \bar{a}_{mnpq} \end{aligned} \quad 96$$

Derivative of the eigentensor $\underline{\underline{q}}$ can be found in Appendix I. Symmetry requirements of the transformed orthotropic tensor reduces the total number of independent non-zero components to 9, and additional special symmetry properties of the exact 4th order tensor requires that $\bar{a}_{ijkl} = \bar{a}_{kjil} = \bar{a}_{ljki} = \bar{a}_{ikjl} = \bar{a}_{ilkj}$ reduces the non-zero independent components to the 6 diagonal terms. i.e.

$$\bar{A}_{ij} = \bar{A}_{kk} \quad \{k : k = 9 - i - j, \quad i \neq j\} \quad 97$$

The normalization property $a_{ijkk} = a_{ij}$ of the exact 4th order tensor further requires that:

$$\begin{bmatrix} \bar{A}_{44} \\ \bar{A}_{55} \\ \bar{A}_{66} \end{bmatrix} = \underline{\underline{D}}^{-1} \left\{ \begin{bmatrix} \lambda_1 \\ \lambda_2 \\ \lambda_3 \end{bmatrix} - \begin{bmatrix} \bar{A}_{11} \\ \bar{A}_{22} \\ \bar{A}_{33} \end{bmatrix} \right\} \quad 98$$

Where, λ_i are the eigenvalues of the 2nd order orientation tensor a_{ij} , $\sum_i \lambda_i = 1$ and $\underline{\underline{D}} = \begin{bmatrix} 0 & 1 & 1 \\ 1 & 0 & 1 \\ 1 & 1 & 0 \end{bmatrix}$.

Based on the foregoing conditions, the only three surviving non-zero independent terms are \bar{A}_{11} , \bar{A}_{22} & \bar{A}_{33} . The general form for orthotropic closure is to express the three surviving non-zero independent components (\bar{A}_{11} , \bar{A}_{22} , \bar{A}_{33}) of the contracted 4th order tensor in the principal reference frame after imposing all symmetric and normalization conditions of the exact 4th order tensor, as a scalar function $F_k(\lambda_1, \lambda_2)$ of the two largest eigenvalues (λ_1, λ_2) of the 2nd order tensor. Most fitted closures take the form of an nth - order binomial function in λ_1 & λ_2 to represents the scalar function i.e.,

$$\bar{A}_{kk} = F_k(\lambda_1, \lambda_2) = f_k^{(n)}(\lambda_1, \lambda_2), \quad \lambda_1 \geq \lambda_2 \geq \lambda_3, \quad k = 1, 2, 3 \quad 99$$

Polynomial order exceeding $n \geq 4$ fall under the class of eigenvalue based optimal fitting (EBOF) closures. Generally, we can represent the function $f_k^{(n)}$ as a tensor product of a constant coefficient matrix $\underline{\underline{C}}^{(n)}$ and a nth order permuted bivariate polynomial vector $\underline{\underline{\Lambda}}^{(n)} = \underline{\underline{\Lambda}}^{(n)}(\lambda_1, \lambda_2)$, i.e.

$$f^{(n)}(\lambda_1, \lambda_2) = \underline{\underline{C}}^{(n)} \underline{\underline{\Lambda}}^{(n)}(\lambda_1, \lambda_2) = C_{kj}^{(n)} \Lambda_j^{(n)}(\lambda_1, \lambda_2) \quad 100$$

Different representation of $\underline{\underline{C}}^{(n)}$ and $\underline{\underline{\Lambda}}^{(n)}$ depending on the polynomial order fit (n) can be found in Appendix II. The derivative of the components of the orthotropic closure with respect to the 2nd order tensor are thus:

$$\frac{\partial \bar{A}_{kk}}{\partial \mathbf{a}_{rs}} = \frac{\partial \bar{A}_k}{\partial \mathbf{a}_{rs}} = C_{kj}^{(n)} \frac{\partial \Lambda_j^{(n)}}{\partial \mathbf{a}_{rs}} = C_{kj}^{(n)} \Lambda'_{jrs} = C_{kj}^{(n)} \tilde{\Lambda}_{jl}^{(n)} \lambda'_{lrs}, \quad k = 1,2,3, \quad l = 1,2 \quad 101$$

The n th order binomial permutation vector $\underline{\underline{\Lambda}}^{(n)}$ and its derivative coefficient matrix $\underline{\underline{\tilde{\Lambda}}}^{(n)}$ for the quadratic closure are given from terms of binomial expansion respectively as

$$\left\{ \begin{array}{l} \Lambda_k^{(n)}(\lambda_1, \lambda_2) = \lambda_1^{i-j} \lambda_2^j \\ \tilde{\Lambda}_{kl}^{(n)} = \frac{\partial \Lambda_k^{(n)}}{\partial \lambda_l} = \begin{cases} (i-j) \cdot \lambda_1^{i-j-1} \lambda_2^j & l = 1 \\ j \cdot \lambda_1^{i-j} \lambda_2^{j-1} & l = 2 \end{cases}, \quad k|k = j + \frac{1}{2}i(i+1), \quad j = 0 \dots i, \quad i = 0 \dots n \end{array} \right. \quad 102$$

For a special case of orthotropic fitted closure called rational ellipsoid closure (REC) by Wetzel and Tucker [41], the scalar function for the 3 independent tensor component is given as

$$F(\lambda_1, \lambda_2) = \frac{f^{(n)}(\lambda_1, \lambda_2)}{f^{(m)}(\lambda_1, \lambda_2)} \quad 103$$

The derivative of the components of the above with respect to the 2nd order tensor based on the quotient rule is thus:

$$\frac{\partial \bar{A}_{kk}}{\partial \mathbf{a}_{rs}} = \frac{1}{[f^{(m)}]^2} \left[f^{(m)} \frac{\partial f^{(n)}}{\partial \mathbf{a}_{rs}} - f^{(n)} \frac{\partial f^{(m)}}{\partial \mathbf{a}_{rs}} \right] \quad 104$$

From normalization condition of the 4th order tensor, we obtain for the derivative of \bar{A}_{kk} , ($k = 4,5,6$)

$$\frac{\partial \bar{A}_{kk}}{\partial \mathbf{a}_{rs}} = D_{ki}^{-1} \left\{ \frac{\partial \lambda_i}{\partial \mathbf{a}_{rs}} - \frac{\partial \bar{A}_{ii}}{\partial \mathbf{a}_{rs}} \right\}, \quad \frac{\partial \lambda_i}{\partial \mathbf{a}_{rs}} = E_{il} \lambda'_{lrs}, \quad \underline{\underline{E}} = \begin{bmatrix} 1 & 0 & -1 \\ 0 & 1 & -1 \end{bmatrix}^T \quad 105$$

$i = 1,2,3, \quad l = 1,2$

For the partial derivative of the eigenvalues with respect to the components of the 2nd order orientation tensor, kindly refer to Appendix I.

(f) Invariant Based Optimal Fitting Closure (IBOF) Approximations

The IBOF closure approximation was developed by Chung et al. [44] and combined the qualities of the natural closure representation of the 4th order closure approximation by Verleye & Dupret [43] and optimal fitting of invariants of the 4th order tensor based on actual flow data obtained from distribution function (DFC) to obtain unknown coefficients similar to the orthotropic fitted closures by Cintra and Tucker [36]. In contracted form the 4th order tensor based on symmetry properties is given as

$$\underline{\underline{A}} = \begin{bmatrix} A_{11} & A_{12} & A_{13} & A_{14} & A_{15} & A_{16} \\ & A_{22} & A_{23} & A_{24} & A_{24} & A_{26} \\ & & A_{33} & A_{34} & A_{35} & A_{36} \\ & & & A_{44} & A_{45} & A_{46} \\ & & & & A_{55} & A_{56} \\ \dots Sym & & & & & A_{66} \end{bmatrix} \quad 106$$

Based on special symmetry requirement.

$$A_{44} = A_{23}, \quad A_{45} = A_{36}, \quad A_{46} = A_{25}, \quad A_{55} = A_{13}, \quad A_{56} = A_{14}, \quad A_{66} = A_{12} \quad 107$$

And from the normalization condition

$$\sum_{n=1}^3 A_{nm} = a_m, \quad a_m = a_{ij}, \quad m = \begin{cases} i = j & i = j \\ 9 - i - j & i \neq j \end{cases} \quad 108$$

Or more explicitly we derive the sets of equations in eqn. 109 below.

$$\begin{aligned} A_{11} + A_{12} + A_{13} &= a_{11} \\ A_{12} + A_{22} + A_{23} &= a_{22} \\ A_{13} + A_{23} + A_{33} &= a_{33} \\ A_{14} + A_{24} + A_{34} &= a_{23} \\ A_{15} + A_{25} + A_{35} &= a_{13} \\ A_{16} + A_{26} + A_{36} &= a_{12} \end{aligned} \quad 109$$

taking partial derivatives of equation [107,& 108] we obtain in indicial representation.

$$\frac{\partial A_{mn}}{\partial a_{rs}} = \frac{\partial A_{ij}}{\partial a_{rs}}, \quad \&, \quad \sum_{n=1}^3 \frac{\partial A_{nm}}{\partial a_{rs}} = \frac{\partial a_m}{\partial a_{rs}} \quad 110$$

There are thus only 9 independent components for the 4th order tensor. The IBOF is developed in terms of the full symmetric 4th order expansion of a_{ijkl} as a combination of the 2nd order tensor a_{ij} and identity matrix δ_{kl} based on Cayley-Hamilton theory is given as

$$\begin{aligned} a_{ijkl} &= \beta_1 S(\delta_{ij}\delta_{kl}) + \beta_2 S(\delta_{ij}a_{kl}) + \beta_3 S(a_{ij}a_{kl}) + \beta_4 S(\delta_{ij}a_{km}a_{ml}) + \beta_5 S(a_{ij}a_{km}a_{ml}) \\ &\quad + \beta_6 S(a_{im}a_{mj}a_{kn}a_{nl}) \end{aligned} \quad 111$$

Where the S operator represents the symmetric permutation expansion of its argument, for example,

$$\begin{aligned} S(T_{ijkl}) &= \frac{1}{24} [T_{ijkl} + T_{ijlk} + T_{ikjl} + T_{iklj} + T_{iljk} + T_{ilkj} + T_{jikl} + T_{jilk} + T_{jkil} + T_{jkli} \\ &\quad + T_{jljk} + T_{jlki} + T_{kijl} + T_{kilj} + T_{kjlj} + T_{kjlj} + T_{kljk} + T_{klji} + T_{lijj} + T_{likj} \\ &\quad + T_{ljik} + T_{ljki} + T_{lkij} + T_{lkji}] \end{aligned} \quad 112$$

We obtain the derivative of the 4th order tensor with respect to components of 2nd order tensor by product rule thus.

$$\begin{aligned}
\frac{\partial}{\partial a_{rs}} \{a_{ijkl}\} = & \left[\frac{\partial \beta_1}{\partial a_{rs}} S(\delta_{ij} \delta_{kl}) + \frac{\partial \beta_2}{\partial a_{rs}} S(\delta_{ij} a_{kl}) + \frac{\partial \beta_3}{\partial a_{rs}} S(a_{ij} a_{kl}) + \frac{\partial \beta_4}{\partial a_{rs}} S(\delta_{ij} a_{km} a_{ml}) \right. \\
& + \frac{\partial \beta_5}{\partial a_{rs}} S(a_{ij} a_{km} a_{ml}) + \left. \frac{\partial \beta_6}{\partial a_{rs}} S(a_{im} a_{mj} a_{kn} a_{nl}) \right] + \dots \\
& + \left[\beta_2 S(\delta_{ij} \delta_{kr} \delta_{ls}) + \beta_3 \{S(\delta_{ir} \delta_{js} a_{kl}) + S(a_{ij} \delta_{kr} \delta_{ls})\} \right. \\
& + \beta_4 \{S(\delta_{ij} \delta_{kr} \delta_{ms} a_{ml}) + S(\delta_{ij} a_{km} \delta_{mr} \delta_{ls})\} \\
& + \beta_5 \{S(\delta_{ir} \delta_{js} a_{km} a_{ml}) + S(a_{ij} \delta_{kr} \delta_{ms} a_{ml}) + S(a_{ij} a_{km} \delta_{mr} \delta_{ls})\} \\
& + \beta_6 \{S(\delta_{ir} \delta_{ms} a_{mj} a_{kn} a_{nl}) + S(a_{im} \delta_{mr} \delta_{js} a_{kn} a_{nl}) + S(a_{im} a_{mj} \delta_{kr} \delta_{ns} a_{nl}) \\
& \left. + S(a_{im} a_{mj} a_{kn} \delta_{nr} \delta_{ls})\} \right]
\end{aligned} \tag{113}$$

The β_i coefficients are expressed as functions of the second and third invariants (II & III) of the 2nd order tensor a_{ij} . Based on normalization condition and full symmetry requirement coupled with the Cayley-Hamilton theorem, there remains only 3 independent coefficients to determine. The expressions for the IBOF dependent coefficients ($\beta_1, \beta_2, \beta_5$) are given as

$$\begin{aligned}
\beta_1 = & \frac{3}{5} \left[-\frac{1}{7} + \frac{1}{5} \beta_3 \left(\frac{1}{7} + \frac{4}{7} \text{II} + \frac{8}{3} \text{III} \right) - \beta_4 \left(\frac{1}{5} - \frac{8}{15} \text{II} - \frac{14}{15} \text{III} \right) + \dots \right. \\
& \left. - \beta_6 \left(\frac{1}{35} - \frac{4}{35} \text{II} - \frac{24}{105} \text{III} + \frac{16}{15} \text{II III} + \frac{8}{35} \text{II}^2 \right) \right] \\
\beta_2 = & \frac{6}{7} \left[1 - \frac{1}{5} \beta_3 (1 + 4\text{II}) + \frac{7}{5} \beta_4 \left(\frac{1}{6} - \text{II} \right) - \beta_6 \left(-\frac{1}{5} + \frac{4}{5} \text{II} + \frac{2}{3} \text{III} - \frac{8}{5} \text{II}^2 \right) \right] \\
\beta_5 = & -\frac{4}{5} \beta_3 - \frac{7}{5} \beta_4 - \frac{6}{5} \beta_6 \left(1 - \frac{4}{3} \text{II} \right)
\end{aligned} \tag{114}$$

We obtain the explicit derivatives of the dependent coefficients via the product rule thus

$$\begin{aligned}
\frac{\partial \beta_1}{\partial a_{rs}} = & \frac{3}{5} \left[\frac{1}{5} \frac{\partial \beta_3}{\partial a_{rs}} \left(\frac{1}{7} + \frac{4}{7} \text{II} + \frac{8}{3} \text{III} \right) - \frac{\partial \beta_4}{\partial a_{rs}} \left(\frac{1}{5} - \frac{8}{15} \text{II} - \frac{14}{15} \text{III} \right) + \dots \right. \\
& \left. - \frac{\partial \beta_6}{\partial a_{rs}} \left(\frac{1}{35} - \frac{4}{35} \text{II} - \frac{24}{105} \text{III} + \frac{16}{15} \text{II III} + \frac{8}{35} \text{II}^2 \right) \right] + \dots + \frac{3}{5} \left[\left[\frac{4}{35} \beta_3 - \beta_4 \right. \right. \\
& \left. \left. + \beta_6 \left(\frac{4}{35} - \frac{16}{35} \text{II} - \frac{16}{15} \text{III} \right) \right] \frac{\partial \text{II}}{\partial a_{rs}} + \left[\frac{18}{53} \beta_3 + \frac{14}{15} \beta_4 + \beta_6 \left(\frac{24}{105} - \frac{16}{15} \text{II} \right) \right] \frac{\partial \text{III}}{\partial a_{rs}} \right] \\
\frac{\partial \beta_2}{\partial a_{rs}} = & \frac{6}{7} \left[-\frac{1}{5} \frac{\partial \beta_3}{\partial a_{rs}} (1 + 4\text{II}) + \frac{7}{5} \frac{\partial \beta_4}{\partial a_{rs}} \left(\frac{1}{6} - \text{II} \right) - \frac{\partial \beta_6}{\partial a_{rs}} \left(-\frac{1}{5} + \frac{4}{5} \text{II} + \frac{2}{3} \text{III} - \frac{8}{5} \text{II}^2 \right) \right] \\
& + \frac{6}{7} \left[-\frac{1}{5} [4\beta_3 + 7\beta_4 + \beta_6(4 - 16\text{II})] \frac{\partial \text{II}}{\partial a_{rs}} - \frac{2}{3} \beta_6 \frac{\partial \text{III}}{\partial a_{rs}} \right] \\
\beta_5 = & -\frac{4}{5} \frac{\partial \beta_3}{\partial a_{rs}} - \frac{7}{5} \frac{\partial \beta_4}{\partial a_{rs}} - \frac{6}{5} \frac{\partial \beta_6}{\partial a_{rs}} \left(1 - \frac{4}{3} \text{II} \right) + \frac{8}{5} \beta_6 \frac{\partial \text{II}}{\partial a_{rs}}
\end{aligned} \tag{115}$$

The independent coefficients ($\beta_3, \beta_4, \beta_6$) by Chung et al. [44] were obtained from a 5th order binomial fitted function in terms of II & III thus:

$$\beta_m = \sum_{i=0}^5 \sum_{j=0}^i a_k^m \cdot \Pi^{i-j} \text{III}^j, \quad k = j + \frac{1}{2}i(i+1) \quad 116$$

Where the coefficients of the binomial terms can be found in Table 17 (Appendix II). The non-unity invariants of a_2 are respectively given as

$$\text{II} = \lambda_1\lambda_2 + \lambda_2\lambda_3 + \lambda_3\lambda_1, \quad \text{III} = \lambda_1\lambda_2\lambda_3 \quad 117$$

The derivative of the independent coefficient with respect to the components of the 2nd order tensor is

$$\frac{\partial \beta_m}{\partial a_{rs}} = \sum_{i=0}^5 \sum_{j=0}^i a_k^m \left\{ (i-j) \cdot \Pi^{i-j-1} \text{III}^j \frac{\partial \text{II}}{\partial a_{rs}} + j \cdot \Pi^{i-j-1} \text{III}^{j-1} \frac{\partial \text{III}}{\partial a_{rs}} \right\} \quad 118$$

where,

$$\begin{aligned} \frac{\partial \text{II}}{\partial a_{rs}} &= (\lambda_2 + \lambda_3) \frac{\partial \lambda_1}{\partial a_{rs}} + (\lambda_1 + \lambda_3) \frac{\partial \lambda_2}{\partial a_{rs}} + (\lambda_1 + \lambda_2) \frac{\partial \lambda_3}{\partial a_{rs}} \\ \frac{\partial \text{III}}{\partial a_{rs}} &= (\lambda_2\lambda_3) \frac{\partial \lambda_1}{\partial a_{rs}} + (\lambda_1\lambda_3) \frac{\partial \lambda_2}{\partial a_{rs}} + (\lambda_1\lambda_2) \frac{\partial \lambda_3}{\partial a_{rs}} \end{aligned} \quad 119$$

Error Estimate

The performance of the Newton-Raphson (NR) method in accurately predicting the steady-state values of the 2nd order orientation tensor component, is accessed based on the relative absolute error between results of the focus NR method and a reference method, in this case the explicit 4th order Runge-Kutta (RK4) numerical method. We define the error percent as

$$err = \frac{a_{mn}^{NR} - a_{mn}^{ref}}{a_{mn}^{ref}} \times 100\% \quad 120$$

Results and Discussion

We present results of validation carried out for the derived partial derivatives of material derivative for the 2nd order tensor with respect to its components for each model and closure approximations discussed in preceding sections using finite differences. We also present result of the validation for the steady state orientation obtained using the Newton Raphson method by comparing with those obtained using the explicit 4th order Runge-Kutta ode method. Validation exercise is carried out for different flow conditions.

1. Validation of Derivatives based on Finite Difference Approximation

The results of the validation based on comparison of the Jacobian obtained with the exact derivative to the finite difference approximation is presented below. We present the error defined as the Euclidean norm of the difference between the results obtained from both methods. i.e.

$$err = \left\| \underline{J}^{exact} - \underline{J}^{FD} \right\|_2 \quad 121$$

The central difference finite difference approximation is used according to

$$J_{mni}^{FD} = \frac{R_{mn}(a_{ij} + \delta a_{ij}) - R_{mn}(a_{ij} - \delta a_{ij})}{2\delta a_{ij}} + O(\delta^2)$$

The model parameters used here can be found in Table 5. The results of the error are shown for different models and closure approximations below. We assume for this validation exercise a ‘randomly’ generated orientation state $\underline{\underline{A}}^0$ given below:

$$\underline{\underline{A}}^0 = \begin{bmatrix} 0.0622 & 0.0765 & 0.0398 \\ 0.0765 & 0.5521 & 0.0186 \\ 0.0398 & 0.0186 & 0.3857 \end{bmatrix}$$

	<u>HYB_1</u>	<u>HYB_2</u>	<u>ISO</u>	<u>LIN</u>	<u>QDR</u>	<u>SF2</u>	<u>HL1</u>	<u>HL2</u>
FT	6.4360e-09	9.3849e-09	2.2195e-09	4.1879e-09	2.6914e-09	2.0949e-08	9.6178e-09	4.3940e-08
PT	8.0880e-09	7.5487e-09	5.8367e-09	5.0032e-09	4.2438e-09	1.6776e-08	8.2414e-09	3.4809e-08
iARD	5.7369e-09	1.2712e-08	3.4444e-09	6.3363e-09	5.7281e-09	5.1004e-09	8.7737e-09	1.6148e-08
pARD	7.1691e-09	5.4745e-09	2.7221e-09	2.4378e-09	4.1547e-09	1.4805e-08	9.8182e-09	3.6185e-08
WPT	8.5633e-09	1.0386e-08	3.7731e-09	2.5253e-09	2.9256e-09	1.4543e-08	9.6324e-09	3.5284e-08
Dz	5.8987e-09	8.2475e-09	2.3728e-09	5.4843e-09	3.2334e-09	7.1374e-09	1.0594e-08	2.7732e-08
NEM	6.4903e-09	9.3064e-09	4.0116e-09	4.3136e-09	1.6118e-09	2.1012e-08	9.8464e-09	4.4062e-08
pARD-RSC	1.0030e-08	1.3343e-08	1.3062e-08	1.0506e-08	1.3699e-08	5.3778e-09	1.3441e-08	1.6482e-08
iARD-RPR	5.6451e-09	6.8998e-09	3.4777e-09	3.6868e-09	5.2224e-09	1.0731e-08	1.0324e-08	2.0512e-08

Table 2: Result of error obtained for different evolution models and different permutation closure approximations.

	<u>IBOF</u>	<u>ORS</u>	<u>ORT</u>	<u>NAT_1</u>	<u>ORW</u>	<u>NAT_2</u>
FT	6.1748e-07	4.5725e-08	3.3508e-08	3.5570e-08	5.9942e-08	5.8124e-08
PT	5.6437e-07	3.3269e-08	2.5174e-08	3.0756e-08	5.6934e-08	3.9459e-08
iARD	4.4942e-07	2.1292e-08	1.9339e-08	2.5119e-08	4.7618e-08	2.6629e-08
pARD	5.5458e-07	3.2158e-08	2.4788e-08	2.9749e-08	5.3542e-08	3.9564e-08
WPT	5.6412e-07	3.4300e-08	2.6217e-08	3.0395e-08	5.7198e-08	4.0679e-08
Dz	6.4226e-07	2.8050e-08	2.9196e-08	3.5323e-08	6.7044e-08	3.2757e-08
NEM	6.1978e-07	4.6150e-08	3.3879e-08	3.6486e-08	6.0619e-08	5.8685e-08
pARD-RSC	4.1821e-07	2.0742e-08	1.8016e-08	2.5292e-08	4.7718e-08	2.7998e-08
iARD-RPR	3.4882e-07	1.6010e-08	1.4040e-08	1.9636e-08	3.6873e-08	1.7086e-08

Table 3: Result of error obtained for different evolution models and different orthotropic fitted and IBOF closure approximations.

	WTZ	LAR32	ORW3	VST	FFLAR4	LAR4
FT	4.3147e-07	5.0800e-07	6.4960e-08	3.1567e-07	4.3188e-07	4.3101e-07
PT	4.0286e-07	4.7162e-07	5.2842e-08	2.9443e-07	4.0435e-07	3.9967e-07
iARD	3.0776e-07	3.6782e-07	4.2132e-08	2.2662e-07	3.0115e-07	3.0665e-07
pARD	3.8741e-07	4.5415e-07	5.2287e-08	2.8548e-07	3.8500e-07	3.8818e-07
WPT	4.0391e-07	4.7234e-07	5.6117e-08	2.9350e-07	4.0486e-07	3.9851e-07
Dz	4.8010e-07	5.5454e-07	6.0103e-08	3.3924e-07	4.8016e-07	4.6691e-07
NEM	4.3254e-07	5.0936e-07	6.5200e-08	3.1653e-07	4.3271e-07	4.3182e-07
pARD-RSC	2.9401e-07	3.4878e-07	4.1548e-08	2.1358e-07	2.9236e-07	2.9070e-07
iARD-RPR	2.4509e-07	2.9082e-07	2.8202e-08	1.7359e-07	2.3590e-07	2.4110e-07

Table 4: Result of error obtained for different evolution models and different EBOF closure approximations.

Validation using explicit 4th-order Runge-Kutta (RK4) Method

In this section, results for the steady state values of the preferred orientation states obtained for various cases using the Newton Raphson algorithm are compared to those obtained based on the 4th order explicit Runge-Kutta method. Three (3) sample cases were studied here, the first set of models are based on study by Falvoro et al [23] and the 2 other model set were based on study by Tseng et al [10]. The EBOF closure approximation of Verweyst [56] has been utilized for all analysis. The following data have been used for the different models considered in the first case study [23].

	C_I	ARD Parameters
FT	0.0311	-
Dz	0.0258	$D_z = 0.051, \hat{n} = [0 \ 0 \ 1]$
iARD	0.0562	$C_M = 09977$
pARD	0.0169	$\Omega = 0.9868$
WPT	0.0504	$w = 0.9950$
MRD	0.0198	$\begin{bmatrix} D_1 & D_2 & D_3 \\ 1.000 & 0.7946 & 0.0120 \end{bmatrix}$
PT	-	$\begin{bmatrix} b_1 & b_2 & b_3 & b_4 & b_5 \\ 1.924 & 58.39 & 400 & 0.1168 & 0 \end{bmatrix} \times 10^{-4}$

Table 5: Case Study 1 parameters for the FT, Dz, iARD, pARD, WPT, MRD and PT models [23]

A random orientation state was considered for the initial tensor in the RK4 while for the NR method we consider an initial guess value $\underline{\underline{A}}^0$ for the 2nd order orientation tensor below.

$$\underline{\underline{A}}^0 = \begin{bmatrix} 0.30 & 0.00 & 0.00 \\ 0.00 & 0.60 & 0.10 \\ 0.00 & 0.10 & 0.10 \end{bmatrix}$$

The transient profiles for the component of the 2nd order orientation tensor based on RK4 method for the models presented in Table 5 are shown in Figure 2 below.

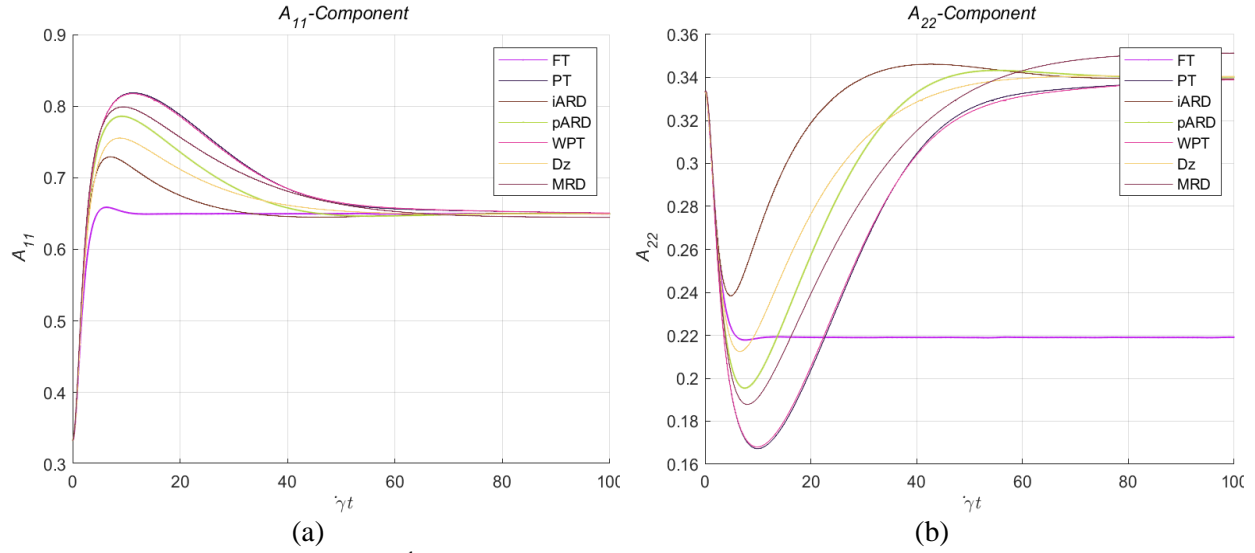


Figure 2 : Time evolution of the 2nd order orientation tensor for calibrated FT, PT, iARD, pARD, WPT, Dz and MRD models for (a) A_{11} component (b) A_{22} component.

Table 6 below shows result of the error estimate of the steady state values of the orientation tensor components obtained by the NR method for the various models considered using the RK4 values as reference. From the result we see the NR predictions are possess good accuracy.

	A_11	A_22	A_13
FT	0.0014	0.0009	0.0053
PT	0.0038	0.0022	0.0067
iARD	0.0032	0.0015	0.0033
pARD	0.0073	0.0035	0.0534
WPT	0.0026	0.0015	0.0099
Dz	0.0297	0.0155	0.0086
MRD	0.0017	0.0009	0.0000

Table 6: Error estimates of the A_{11} , A_{22} & A_{13} steady-state orientation tensor component values for FT, Dz, iARD, pARD, WPT, MRD and PT models

The second case study is based on work by Tseng et al. [10], the calibrated data based on the different model improvements for slow orientation kinetics which they utilized are presented in Table 7 below.

	FT	SRF	RSC	RPR
C_I	0.01	0.01	0.01	0.01
κ	—	0.1	0.1	—
α	—	—	—	0.9
β	—	—	—	0

Table 7: Case Study 2 parameters for the FT, SRF, RSC and RPR models [10]

A random orientation state was used as the starting orientation for the RK4 analysis while the initial guess $\underline{\underline{A}}^0$ given below was used for the Newton Raphson method.

$$\underline{\underline{A}}^0 = \begin{bmatrix} 0.35 & 0.00 & 0.00 \\ 0.00 & 0.55 & 0.10 \\ 0.00 & 0.10 & 0.10 \end{bmatrix}$$

Two flow cases were considered:

1. Simple shear flow in the 1-2 plane, $L_{12} = \dot{\gamma}$ (L1).
2. Balanced shear/planar-elongation flow, simple shear in 1-2 plane superimposed on planar elongation in 1-2 plane. $L_{11} = -\dot{\epsilon}, L_{22} = \dot{\epsilon}, L_{12} = \dot{\gamma}$ given $\dot{\gamma}/\dot{\epsilon} = 10$ (L2).

The time evolution of the components of the 2nd order orientation tensor based on the RK4 method are shown in Figure 3 below.

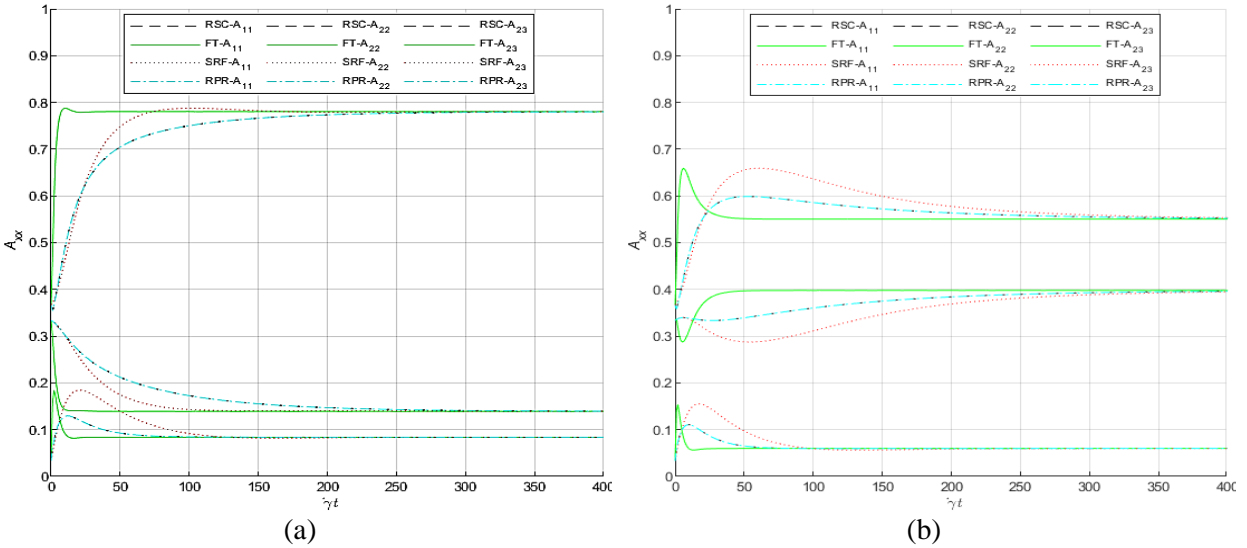


Figure 3 : Time evolution of the A_{11}, A_{22} & A_{13} components of the 2nd order orientation tensor for calibrated FT, SRF, RSC and FT-RPR models for (a) simple shear flow and (b) shearing/stretching combination flow.

The percentage error estimate between the NR steady state values and the reference RK4 values are presented in Table 8 below. Results show a high level in accuracy in prediction based on the NR method.

	A_11_L1	A_22_L1	A_13_L1	A_11_L2	A_22_L2	A_13_L2
RSC	0.0000	0.0000	0.0000	0.0003	0.0007	0.0167
FT	0.0022	0.0021	0.0263	0.0005	0.0009	0.0017
SRF	0.0022	0.0013	0.0048	0.0075	0.0085	0.0167
RPR	0.0000	0.0000	0.0000	0.0000	0.0002	0.0033

Table 8: Error estimates of the A_{11}, A_{22} & A_{13} steady-state orientation tensor component values for RSC, FT, SRF, and RPR models and for the 2 different flow fields (L1 & L2)

In the third case, we consider more complex model development usually involving the combination of two models typically found in injection molding simulation packages such as Moldex3D. The different cases are based on [10] and the model parameter used for the analysis are given in Table 9, & Table 10 below.

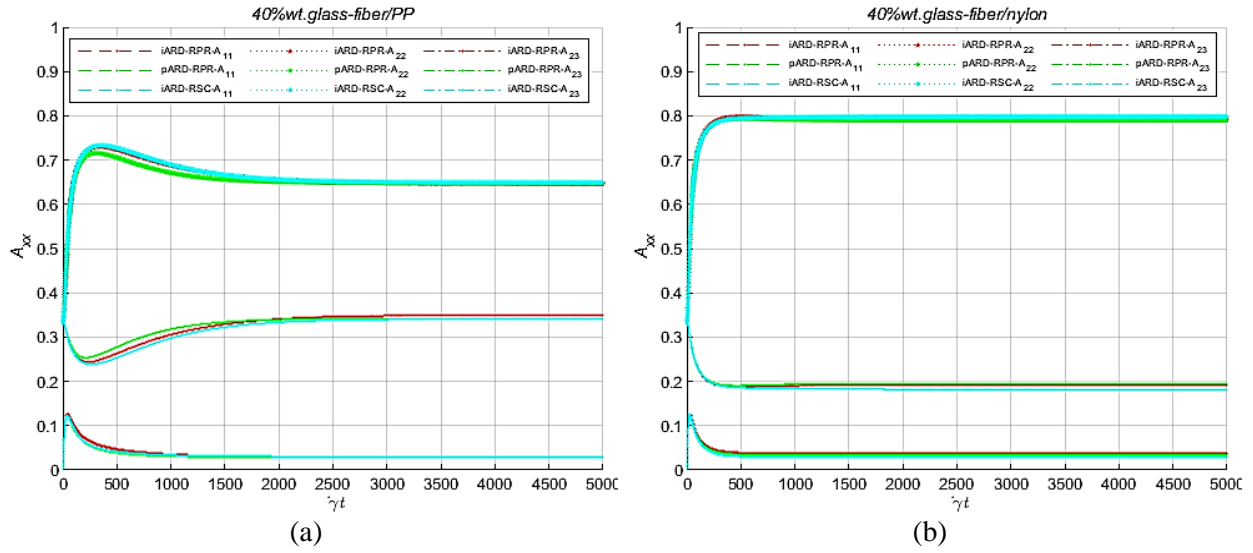
We assume a random initial orientation state for the reference RK4 method and the same initial guess as with case study 2 for the NR method. The result of the steady state values based on the RK4 method for the different methods are shown in Figure 4. The percentage error estimate of the NR steady state values with respect to the RK4 reference values are given in Table 11 and the results show negligible discrepancy in values obtained.

	40 wt. % glass-fiber/PP	31 wt. % carbon-fiber/PP	40 wt. % glass-fiber/nylon
κ	1/30	1/30	1/20
b_1	3.842×10^{-4}	3.728×10^{-3}	4.643×10^{-4}
b_2	-1.786×10^{-3}	-1.695×10^{-2}	-6.169×10^{-4}
b_3	5.250×10^{-2}	1.750×10^{-1}	1.900×10^{-2}
b_4	1.168×10^{-5}	-3.367×10^{-3}	9.650×10^{-4}
b_5	-5.000×10^{-4}	-1.000×10^{-2}	7.000×10^{-4}

Table 9: ARD-RSC Parameters [10]

	40 wt. % glass-fiber/PP	31 wt. % carbon-fiber/PP	40 wt. % glass-fiber/nylon
C_I	0.0165	0.0630	0.0060
C_M	0.999	1.010	0.900
Ω	0.988	0.965	0.900
α	0.965	0.965	0.950
β	0	0	0

Table 10: *iARD-RPR* & *pARD-RPR* Parameters [10]



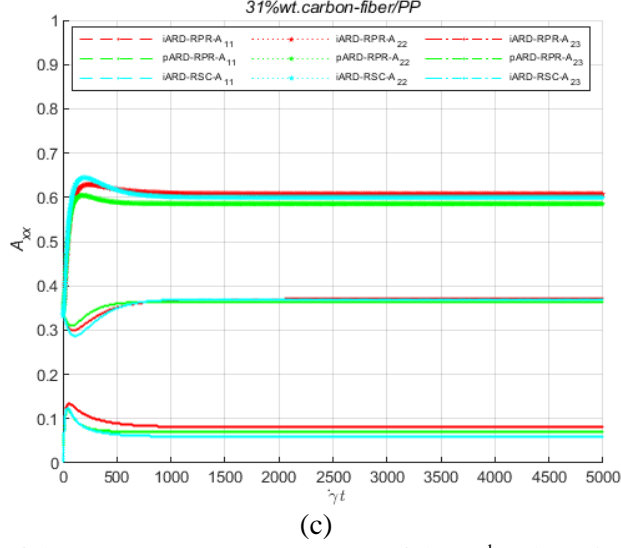


Figure 4 : Time evolution of the A_{11} , A_{22} & A_{13} components of the 2nd order orientation tensor for calibrated iARD-RPR, iARD-RSC, pARD-RPR models for (a) 40% wt. glass-fiber/PP (b) 40% wt. glass-fiber/nylon (c) 31% wt. carbon-fiber/PP

The results shown in Table 11 reveals good performance in terms of accuracy for the NR method based on the calculated error estimates of the steady state orientation values for the 3-tensor components and for the various models.

	<u>A_11</u>	<u>A_22</u>	<u>A_13</u>
iARD-RPR1	0.0060	0.0032	0.0036
pARD-RPR1	0.0009	0.0006	0.0311
iARD-RSC1	0.0070	0.0037	0.0134
iARD-RPR2	0.0003	0.0002	0.0012
pARD-RPR2	0.0003	0.0007	0.0156
iARD-RSC2	0.0008	0.0017	0.0551
iARD-RPR3	0.0000	0.0001	0.0053
pARD-RPR3	0.0000	0.0001	0.0059
iARD-RSC3	0.0066	0.0014	0.0067

Table 11: Error estimates of the A_{11} , A_{22} & A_{13} steady-state orientation tensor component values for iARD-RPR, iARD-RSC, pARD-RPR models for (1) 40% wt. glass-fiber/PP (2) 40% wt. glass-fiber/nylon (3) 31% wt. carbon-fiber/PP

Performance of the different Closure Approximations

The performance of the NR method in obtaining the steady state values for different closure approximations of the 4th order orientation tensor in terms of accuracy and stability has also been assessed. We consider for this assessment the FT model with a $C_I = 0.01$. The initial orientation state for the RK4 reference method is assumed to be random and we assume the same initial guess for the NR method as that of the preceding section. From Table 12, except for the HL2 closure approximation all other Hinch and Leal closures behaved well. By reason of the inherent nature of the transient behavior of the orientation tensor based on

the HL2 closure approximation which shows a sudden transition in steady state values at a time fraction of about 100 (Figure 5), we observe a discrepancy in the result for this closure since the NR method has no memory of the history of the orientation state and the accuracy of its prediction is based on the initial guess. The NR method predicts the initial steady state values of $A_{11} = 0.6103, A_{12} = 0.0206$ while the RK4 method transitions to a final steady state orientation of $A_{11} = 0.5759, A_{12} = 0.0467$. The higher order fitted closure approximations behave well in the NR methods and show good accuracy in predictions (Table 13).

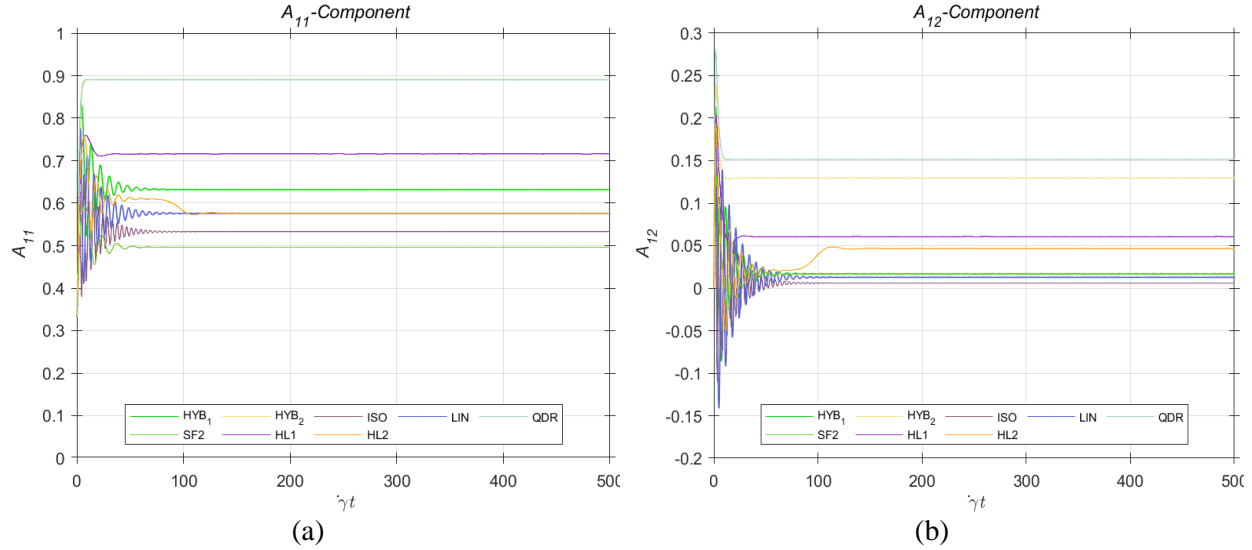


Figure 5 : Transient profiles of 2nd order orientation tensor evolution for (a) component A_{11} and (b) component A_{12} for the various Hinch and Leal closure approximations of the 4th order orientation tensor.

	<u>A_11</u>	<u>A_22</u>	<u>A_12</u>
HYB_1	0.0000	0.0005	0.2306
HYB_2	0.0151	0.0017	0.0223
ISO	0.0000	0.0049	0.6305
LIN	0.0004	0.0003	0.4655
QDR	0.0036	0.0006	0.0053
SF2	0.0027	0.0101	0.0419
HL1	0.0042	0.0059	0.0313
HL2	25.9705	5.9662	55.8952

Table 12: Error estimates of the A_{11}, A_{22} & A_{12} steady-state orientation tensor component values based on the various Hinch and Leal closure approximations of the 4th order orientation tensor.

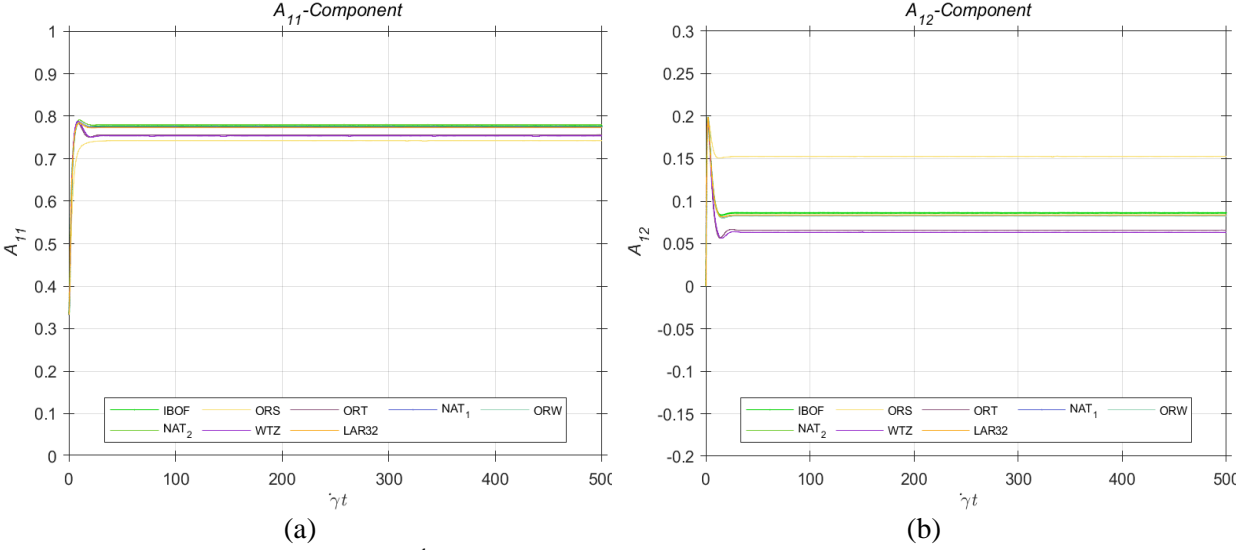


Figure 6 : Transient profiles of 2nd order orientation tensor evolution for (a) component A_{11} and (b) component A_{12} for the higher order orthotropic fitted, IBOF and EBOF closure approximations of the 4th order orientation tensor.

	A_11	A_22	A_12
IBOF	0.0007	0.0015	0.0232
ORS	0.0050	0.0055	0.0151
ORT	0.0781	0.0415	0.1600
NAT_1	0.0000	0.0004	0.0096
ORW	0.0007	0.0001	0.0061
NAT_2	0.0022	0.0017	0.0131
WTZ	0.0000	0.0003	0.0079
LAR32	0.0046	0.0013	0.0203
ORW3	0.0013	0.0003	0.0036
VST	0.0257	0.0123	0.0240
FFLAR4	0.0068	0.0029	0.0327
LAR4	0.0020	0.0008	0.0036

Table 13: Error estimates of the A_{11}, A_{22} & A_{12} steady-state orientation tensor component values based on the higher order fitted closure approximations of the 4th order orientation tensor.

Homogenous Flow Considerations

We consider different homogenous flows to ensure the stability of the Newtons method in finding stable roots. The following flows were considered:

- (i) Simple Shear, $L_{12} = \dot{\gamma}$
- (ii) Two Stretching/Shearing flow, simple shear in 1-2 plane superimposed with uniaxial elongation in 3-direction. $L_{11} = -\dot{\epsilon}$, $L_{22} = \dot{\epsilon}$, $L_{33} = 2\dot{\epsilon}$, $L_{12} = \dot{\gamma}$. Two cases consider, balanced shear/stretch, $\dot{\gamma}/\dot{\epsilon} = 10$, dominant stretch, $\dot{\gamma}/\dot{\epsilon} = 1$
- (iii) Uniaxial Elongation, $L_{11} = 2\dot{\epsilon}$, $L_{22} = L_{33} = -\dot{\epsilon}$

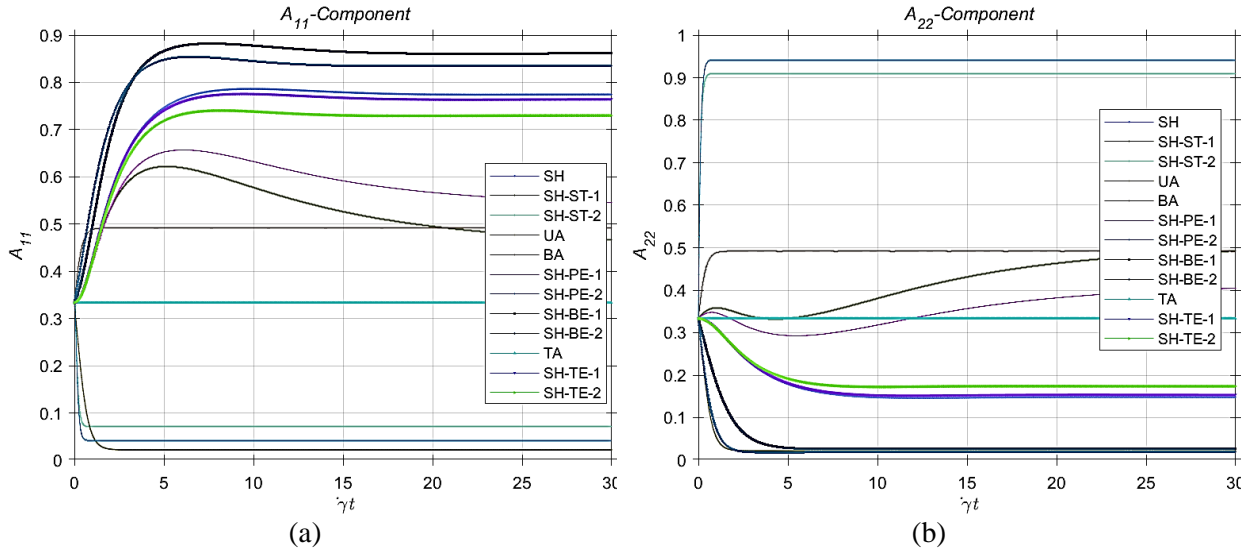
- (iv) Biaxial Elongation, $L_{11} = L_{22} = \dot{\epsilon}$, $L_{33} = -2\dot{\epsilon}$
- (v) Two shear/planar-elongation flow, simple shear in 1-3 plane superimposed on planar elongation in 1-2 plane. $L_{11} = -\dot{\epsilon}$, $L_{22} = \dot{\epsilon}$, $L_{12} = \dot{\gamma}$. Two cases consider, balanced shear-planar elongation, $\dot{\gamma}/\dot{\epsilon} = 10$, & dominant planar elongation, $\dot{\gamma}/\dot{\epsilon} = 1$
- (vi) Balanced shear/bi-axial elongation flow, simple shear in 1-3 plane superimposed on biaxial elongation. $L_{11} = \dot{\epsilon}$, $L_{22} = \dot{\epsilon}$, $L_{12} = \dot{\gamma}$, $L_{33} = -2\dot{\epsilon}$, A range for $\dot{\gamma}$ is used such that, $2 \leq \dot{\gamma}/\dot{\epsilon} \leq 5$
- (vii) Triaxial Elongation, $L_{11} = L_{22} = L_{33} = \dot{\epsilon}$
- (viii) Balanced shear/tri-axial elongation flow, simple shear in 1-3 plane superimposed on biaxial elongation. $L_{11} = \dot{\epsilon}$, $L_{22} = L_{33} = \dot{\epsilon}$, $L_{12} = \dot{\gamma}$, A range for $\dot{\gamma}$ is used such that, $2 \leq \dot{\gamma}/\dot{\epsilon} \leq 5$

The initial orientation state for the RK4 reference method is assumed to be random and the initial guess $\underline{\underline{A}}^0$ assumed for each flow consideration is presented in Table 14 below.

(i)			(ii) & (v)			(iii)			(iv, vii & viii)			(vi)		
0.35	0.00	0.00	0.70	0.00	0.00	0.10	0.00	0.00	0.40	0.00	0.00	0.20	0.00	0.00
0.00	0.55	0.00	0.00	0.20	0.00	0.00	0.10	0.00	0.00	0.40	0.00	0.00	0.70	0.00
0.00	0.00	0.10	0.00	0.00	0.10	0.00	0.00	0.80	0.00	0.00	0.20	0.00	0.00	0.10

Table 14: NR initial guess values for different flow conditions

Among all closure approximations, the natural closure approximations (exact midpoint fit and extended quadratic fit cf. Kuzmin et. al), and the rational ellipsoid (Wetzel) closures behaved well in all flows while the other orthotropic closures had stability issues for one or more of the complex flows and gave non-physical roots. The ability of the NR method to predict accurate results depends on a reasonable initial guess based on the flow type and a suitable closure approximation.



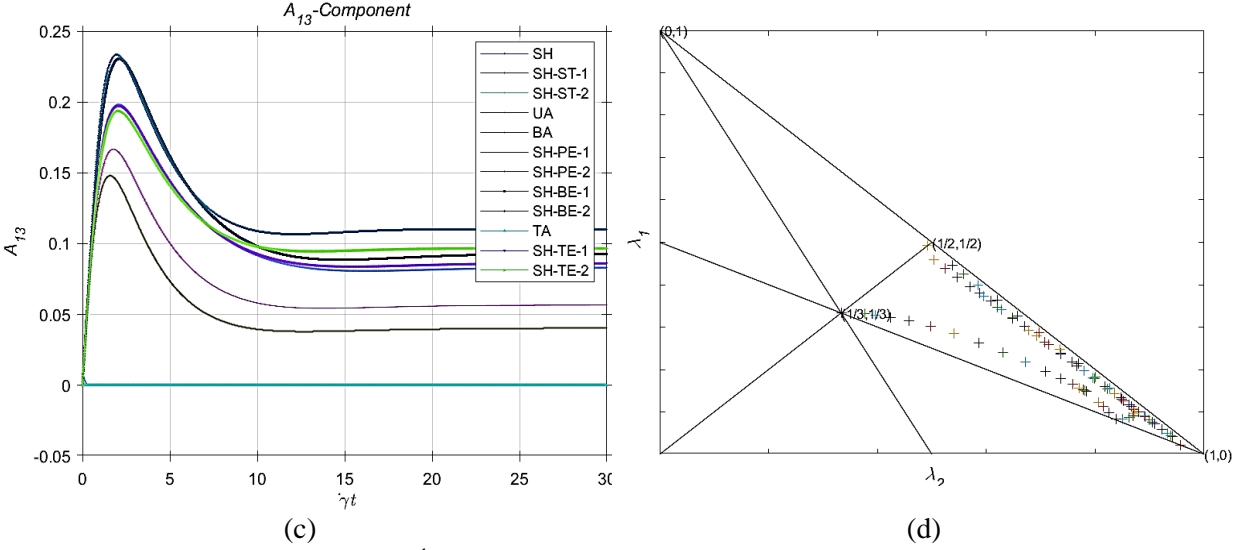


Figure 7 : Transient profiles of 2nd order orientation tensor evolution for (a) component A_{11} and (b) component A_{22} (c) component A_{12} for the various flow considerations. (d) shows the eigenspace for the steady state values obtained for the different flow conditions based on NR method.

	A_11	A_22	A_13
SH	0.0027	0.0014	0.0012
SH-ST-1	0.0004	0.0004	0.0073
SH-ST-2	0.0001	0.0000	0.0000
UA	0.0046	0.0046	0.0000
BA	0.0175	0.0175	0.0000
SH-PE-1	0.0019	0.0013	0.0053
SH-PE-2	0.0004	0.0024	0.1631
SH-BE-1	0.0148	0.0003	0.0000
SH-BE-2	0.0053	0.0000	0.0000

Table 15: Error estimates of the A_{11} , A_{22} & A_{12} steady-state orientation tensor component values for the various flow considerations.

Center Gated Disk Flow

The center gated disk flow which is a pressure driven axisymmetric radial flow between parallel plates and typical employed in injection molding simulations has also been considered. Although the flow is steady, the velocity assumes the form of a uniform source flow and is never fully developed but asymptotically approaches zero. Since the velocity gradient is a function of radial distance, the material derivative has an extra variable r in addition to the independent components of the orientation tensor. The Newton Raphson Jacobian is thus modified to incorporate partial derivatives of the residual with respect to the radial distance. Complete derivations of the Jacobian for different models can be found in Appendix xx. For this study, the 40 wt. % glass-fiber/PP parameters found in section xx for the *ARD-RSC*, *iARD-RPR* and *pARD-RPR* have been used. A random orientation state was used as the starting orientation for the RK4 analysis while the initial guess $\underline{\underline{A}}^0$ for the Newton Raphson method was given as

$$\underline{A}^0 = \begin{bmatrix} 0.20 & 0.00 & 0.00 \\ 0.00 & 0.60 & -0.05 \\ 0.00 & 0.00 & 0.00 \end{bmatrix}$$

A large enough radial distance is given such that the flow conditions and the resulting orientation kinematics are quasi-stable, and the NR method determines the orientation components at that radial location. For this study we chose $r/h = 1000$ where $2h$ is the gap thickness. A volume flow rate $Q = 100 \text{ cm}^3/\text{s}$ [19] was used.

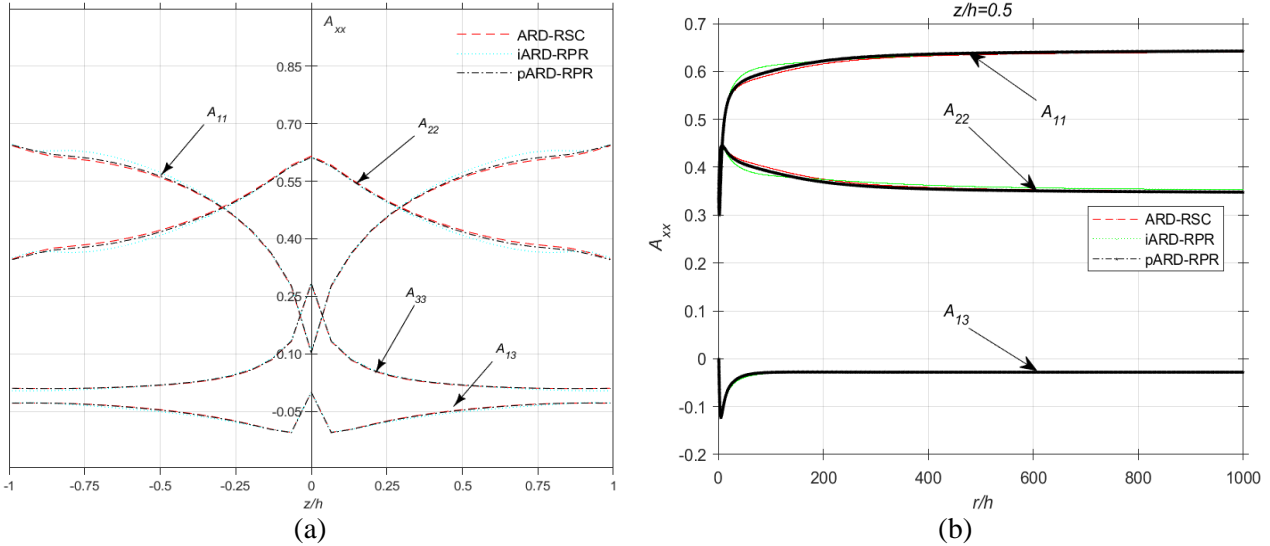


Figure 8 : Flow 2nd order orientation tensor components profiles (a) along transverse section of the flow at a radial distance $r/h = 30$, (b) along radial direction at a height of $z/h = 0.5$.

We observe good alignment in the results of the RK4 and NR method from the results of the percentage error estimate in Table xx below.

	A_11	A_22	A_13
ARD-RSC	0.0800	0.0418	0.0857
iARD-RPR	0.0814	0.0443	0.0914
pARD-RPR	0.0539	0.0281	0.0417

Table 16: Error estimates of the A_{11}, A_{22} & A_{12} steady-state orientation tensor component values for the center-gated disk flow.

Conclusion

In conclusion, a Newton-Raphson method has been successfully implemented in determining the steady state 2nd order orientation tensor component values by determining exact partial derivatives of the material derivative of the orientation tensor with respect to its individual components. Different macroscopic fiber orientation moment-tensor models and closure approximations of the 4th order orientation tensor has also considered and the performance of the NR method in different flows have been studied. Like with any typical application of the NR root finding method, a good initial guess of the steady state orientation is required to yield non-physical values. The numerical stability of the NR method depends on complexity of

the flow and the closure approximations. The Natural orthotropic and the IBOF closure approximations performed best for very complex flows. The NR method is comparatively faster compared to the RK4 method. Although obtaining exact derivatives of the 2nd order moment-tensor equation of change can be very cumbersome, once they are modelled, they are computationally more efficient since they require less function evaluations compared to a higher order finite difference method of matching accuracy. Moreover, round off error and truncation error may become significant when dealing with relatively small quantities like the center gated disk flow with velocity gradient asymptotically approaching zero and the finite difference approximation give unstable results.

Appendix I. Eigenvalues and Eigenvector Derivatives [52]

The eigenvalue definition for any system is typically given in terms of the eigen-values λ^k and corresponding eigen-vectors $\underline{\Phi}^k$ as [52]

$$\left[\underline{K} - \lambda_k \underline{M} \right] \underline{\Phi}^k = \underline{F}^k \quad 123$$

For most undamped systems, $\underline{F}^k = \mathbf{0}$, and since $\underline{\Phi}^k \neq \mathbf{0}$ to yield non-trivial solutions, then by setting $\left[\underline{K} - \lambda_k \underline{M} \right] = 0$, we can obtain solutions for λ^k . By reason of the nature of the system matrix $[K_{mn} - \lambda^k M_{mn}]$ being rank deficient with one order less than the matrix size one may adopt a scaling algorithm to obtain the corresponding eigen-vectors $\underline{\Phi}^k$ usually by defining a Mode *I* normalization technique for scaling the eigen-vectors $\underline{\Phi}^k$ via a scalar functions $G^k(\underline{\Phi}^k)$ such that $G^k = 0$, which may be non-linear in nature. The eigenvectors are thus obtained by replacing the n^{th} row of the residual column vector $R_i^k = (K_{ij} - \lambda^k M_{ij})\Phi_j^k - F_i^k$ with $G^k(\underline{\Phi}^k)$ and solving for $\underline{\Phi}^k$ from the equation $\underline{R}^k(\underline{\Phi}^k) = 0$ through any iterative algorithm or explicit solvers. Here we employ the Newton-Raphson's method to obtain $\underline{\Phi}^k$ such that:

$$\underline{\Phi}^{k+} = \underline{\Phi}^{k-} - \underline{J}^{k-1} R^k \quad 124$$

$$R_i^k = \begin{cases} S_{ij}^k \Phi_j^k - F_i^k, & i \neq n \\ G^k(\underline{\Phi}^k), & i = n \end{cases} \quad 125$$

$$J_{ij}^k = \frac{\partial R_i^k}{\partial \Phi_j^k} = \begin{cases} S_{ij}^k, & i \neq n \\ \frac{\partial G^k}{\partial \Phi_j^k}, & i = n \end{cases} \quad 126$$

where

$$S_{ij}^k = K_{ij} - \lambda^k M_{ij} \quad 127$$

The derivative of the eigen values with respect to components \underline{a} can thus be obtained by differentiating eqn. xx assuming symmetry of system matrix, i.e., $S_{ij}^k = S_{ji}^k$ such that:

$$\Phi_i^k \frac{\partial S_{ij}^k}{\partial a_{rs}} \Phi_j^k + F_i^k \frac{\partial \Phi_i^k}{\partial a_{rs}} - \Phi_i^k \frac{\partial F_i^k}{\partial a_{rs}} = 0 \quad 128$$

$$\Phi_i^k S_{ij}^k = S_{ji}^k \Phi_j^k = S_{ij}^k \Phi_j^k = F_i^k \quad 129$$

where:

$$\frac{\partial S_{ij}^k}{\partial a_{rs}} = \frac{\partial K_{ij}}{\partial a_{rs}} - \frac{\partial \lambda^k}{\partial a_{rs}} M_{ij} - \lambda^k \frac{\partial M_{ij}}{\partial a_{rs}} \quad 130$$

Since $\underline{F}_i^k = 0$ for undamped systems

$$\frac{\partial \lambda^k}{\partial a_{rs}} = \frac{1}{(\Phi_i^k M_{ij} \Phi_j^k)} \left\{ \Phi_i^k \left[\frac{\partial K_{ij}}{\partial a_{rs}} - \lambda^k \frac{\partial M_{ij}}{\partial a_{rs}} \right] \Phi_j^k \right\} \quad 131$$

Consequently, we can obtain the corresponding derivatives $\partial \Phi_i^k / \partial a_{rs}$ given $\partial \lambda^k / \partial a_{rs}$ from

$$S_{ij}^k \frac{\partial \Phi_i^k}{\partial a_{rs}} = - \frac{\partial S_{ij}^k}{\partial a_{rs}} \Phi_j^k \quad 132$$

Recalling the system matrix $[\underline{K} - \lambda^k \underline{M}]$ is inherently singular, we can substitute an n^{th} row of the above equation adopting one the normalization techniques with the equation [52]:

$$\frac{\partial G^k}{\partial \Phi_j^k} \frac{\partial \Phi_j^k}{\partial a_{rs}} = \frac{\partial G^k}{\partial a_{rs}} \quad 133$$

The modified differential equation can be recast as given in equation xx below allowing the inversion of the modified system matrix.

$$J_{ij}^k \frac{\partial \Phi_i^k}{\partial a_{rs}} = \frac{\partial Q_i^k}{\partial a_{rs}} \quad 134$$

where:

$$\frac{\partial Q_i^k}{\partial a_{rs}} = \begin{cases} - \frac{\partial G^k}{\partial a_{rs}}, & i = n \\ - \frac{\partial S_{ij}^k}{\partial a_{rs}} \Phi_j^k, & i \neq n \end{cases} \quad 135$$

Smith et. al [52] presents 3 common Mode I normalization techniques thus:

1. Mass Normalization

$$G^k(\underline{\Phi}^k) = \Phi_i^k M_{ij} \Phi_j^k - 1, \quad \frac{\partial G^k}{\partial \Phi_j^k} = 2 \Phi_i^k M_{ij}, \quad \frac{\partial G^k}{\partial a_{rs}} = \Phi_i^k \frac{\partial M_{ij}}{\partial a_{rs}} \Phi_j^k \quad 136$$

2. Preassigning an m^{th} Component of $\underline{\Phi}^k$

$$G^k(\underline{\Phi}^k) = \delta_{mj} \Phi_j^k - \alpha, \quad \frac{\partial G^k}{\partial \Phi_j^k} = \delta_{mj}, \quad \frac{\partial G^k}{\partial a_{rs}} = 0 \quad 137$$

3. Predefining the Euclidean norm of $\underline{\Phi}^k$

$$G^k(\underline{\Phi}^k) = \sqrt{\Phi_j^k \Phi_j^k} - \beta, \quad \frac{\partial G^k}{\partial \Phi_j^k} = \Phi_j^k, \quad \frac{\partial G^k}{\partial a_{rs}} = 0 \quad 138$$

A more direct and efficient approach by Nelson [53] which utilizes mass normalization technique is given below:

$$\frac{\partial \Phi_i^k}{\partial a_{rs}} = V_i^k + c^k \Phi_i^k, \quad c^k = -\Phi_i^k M_{ij} V_j^k - \frac{1}{2} \Phi_i^k \frac{\partial M_{ij}}{\partial a_{rs}} \Phi_j^k, \quad V_i^k = \{ \underline{\underline{SP}}^{k-1} \}_{ij} \frac{\partial QP_j^k}{\partial a_{rs}} \quad 139$$

Given a pre-selected fixed index – m and noting in equation 140-141 below that repeated indices do not imply a summation,

$$SP_{ij}^k = (K_{ij} - \lambda^k M_{ij})(1 - \delta_{mi})(1 - \delta_{mj}) + \delta_{mi} \delta_{mj} \quad 140$$

$$\frac{\partial QP_i^k}{\partial a_{rs}} = -\frac{\partial S_{ij}^k}{\partial a_{rs}} \Phi_j^k (1 - \delta_{mi}) \quad 141$$

Appendix II. Optimal Fitted Closure Approximation Constants/Coefficients

1. Eigenvalue Based Optimal Fitting Closure (EBOF) Approximation

We consider 4 fitted closures approximations of this form. Linear, quadratic, cubic and quartic binomial fitted closures with $(n + 1)(n + 2)/2$ number of parameters and their constants below.

i) Linear Orthotropic Fitted Closure ($n = 1$)

For the general linear orthotropic closure, the constant coefficient matrix $\underline{\underline{C}}'$ is given as

$$\underline{\underline{C}}^{(1)} = \frac{1}{7} \begin{bmatrix} -3/5 & 6 & 0 \\ -3/5 & 0 & 6 \\ 27/5 & -6 & -6 \end{bmatrix}$$

And for the smooth orthotropic closure by Cintra and Tucker (cf. [1]), the constant coefficient matrix $\underline{\underline{C}}'$ is given as

$$\underline{\underline{C}}^{(1)} = \begin{bmatrix} -0.15 & 1.15 & -0.10 \\ -0.15 & 0.15 & 0.90 \\ 0.60 & -0.60 & -0.60 \end{bmatrix}$$

ii) Quadratic Orthotropic Fitted Closures ($n = 2$)

The simple general orthotropic quadratic closure has constant coefficient matrix $\underline{\underline{C}}'$ given as

$$\underline{\underline{C}}^{(2)} = \begin{bmatrix} 0 & 0 & 0 & 1 & 0 & 0 \\ 0 & 0 & 0 & 0 & 0 & 1 \\ 1 & -2 & -2 & 1 & 2 & 1 \end{bmatrix}$$

The orthotropic natural closure - exact midpoint fit [39] has constant coefficient matrix $\underline{\underline{C}}'$ given as

$$\underline{\underline{C}}^{(2)} = \begin{bmatrix} 0.0708 & 0.3236 & -0.3776 & 0.6056 & 0.4124 & 0.3068 \\ 0.0708 & -0.2792 & 0.2252 & 0.2084 & 0.4124 & 0.7040 \\ 1.1880 & -2.0136 & -2.1264 & 0.8256 & 1.7640 & 0.9384 \end{bmatrix}$$

The orthotropic fitted closure by Cintra and Tucker (ORF) (cf. [36]), the constant coefficient matrix $\underline{\underline{C}}'$ is given as

$$\underline{\underline{C}}^{(2)} = \begin{bmatrix} 0.060964 & 0.371243 & -0.369160 & 0.555301 & 0.371218 & 0.318266 \\ 0.124711 & -0.389402 & 0.086169 & 0.258844 & 0.544992 & 0.796080 \\ 1.228982 & -2.054116 & -2.260574 & 0.821548 & 1.819756 & 1.053907 \end{bmatrix}$$

The improved orthotropic fitted closure (ORW2) by Chung and Kwon (cf. [38]), has constant coefficient matrix $\underline{\underline{C}}'$ given as

$$\underline{\underline{C}}^{(2)} = \begin{bmatrix} 0.070055 & 0.339376 & -0.396796 & 0.590331 & 0.411944 & 0.333693 \\ 0.115177 & -0.368267 & 0.094820 & 0.252880 & 0.535224 & 0.800181 \\ 1.249811 & -2.148297 & -2.290157 & 0.898521 & 1.934914 & 1.044147 \end{bmatrix}$$

iii) Cubic Orthotropic Fitted Closures ($n = 3$)

The orthotropic natural closure - extended quadratic fit though of cubic order is essentially quadratic.

a) Non-rational Fitted Closure

The constant coefficient matrix $\underline{\underline{C}}^{(3)}$ for this closure approximation is given as

$$\underline{\underline{C}}^{(3)} = \begin{bmatrix} 0 & 0.5 & 0 & 0.5 & -0.6 & 0 & 0.6 & 0.6 & 0 \\ 0 & 0 & 0.5 & 0 & -0.6 & 0.5 & 0 & 0.6 & 0.6 & 0 \\ 1 & -1.5 & -1.5 & 0.5 & 0.4 & 0.5 & 0 & 0.6 & 0.6 & 0 \end{bmatrix}$$

For the improved 3rd order orthotropic fitted closure ORW3 by Chung and Kwon [38], the constant coefficient matrix is given as

$$[\underline{\underline{C}}^{(3)}]^T = \begin{bmatrix} -0.1480648093 & -0.2106349673 & 0.4868019601 \\ 0.8084618453 & 0.9092350296 & 0.5776328438 \\ 0.7765597096 & 1.1104441966 & 0.4605743789 \\ 0.3722003446 & -1.2840654776 & -2.2462007509 \\ -1.7366749542 & -2.5375632310 & -4.8900459209 \\ -1.3431772379 & 0.1260059291 & -1.9088154281 \\ -0.0324756095 & 0.5856304774 & 1.1817992322 \\ 0.8895946393 & 1.9988098293 & 4.0544348937 \\ 1.7367571741 & 1.4863151577 & 3.8542602127 \\ 0.6631716575 & -0.0756740034 & 0.9512305286 \end{bmatrix}$$

b) Rational Fitted Closure

The rational ellipsoid fitted closure has two permutation vectors, the denominator being one order less than the numerator, i.e., $m = n - 1$ which is of cubic order, $n = 3$

The corresponding constant coefficient matrix for the Wetzel [Ref xx] numerator ($n = 3$) is

$$[\underline{\underline{C}}^{(3)}]^T = \begin{bmatrix} 0.1433751825 & 0.1433751825 & 0.9685744898 \\ -0.6566650339 & -0.5209453949 & -2.5526857671 \\ -0.5106016916 & -0.6463213306 & -2.5756669706 \\ 3.5295952199 & 0.6031924921 & 2.2044050704 \\ 4.4349137241 & 2.3303190917 & 4.4520903005 \\ 0.1229618909 & 5.1539592511 & 2.2485545147 \\ -2.9144388828 & -0.2256222796 & -0.6202937932 \\ -5.5556896198 & -1.6481269200 & -1.8811803355 \\ -2.8284365891 & -5.4494528976 & -1.9023485762 \\ 0.2292109036 & -3.7461520908 & -0.6414620339 \end{bmatrix}$$

And for the denominator ($m = n - 1 = 2$)

$$[\underline{\underline{C}}^{(2)}]^T = \begin{bmatrix} 1.0000000000 & 1.0000000000 & 1.0000000000 \\ 0.7257989503 & 0.6916858207 & -1.2134964928 \\ 3.0941511876 & 3.1282643172 & -1.2128608265 \\ -1.6239324646 & -1.5898193351 & 0.2393747647 \\ -4.7303686308 & -4.7303686308 & 0.6004510415 \\ -3.1742364608 & -3.2083495904 & 0.2162486576 \end{bmatrix}$$

For the LAR32 closure by Mullens [42] the corresponding constant coefficient matrix for the numerator ($n = 3$) is

$$\underline{\underline{C}}^{(3)T} = \begin{vmatrix} 0.087602233 & 0.156805152 & 1.072423739 \\ 0.028205550 & -0.577818864 & -2.803554028 \\ -0.426784335 & -0.514280920 & -2.661576129 \\ 1.274677110 & 0.684250887 & 2.389379765 \\ 0.876469059 & 2.132305029 & 4.566728489 \\ 0.602031647 & 3.454835266 & 2.097523143 \\ -1.066583115 & -0.263237143 & -0.658248930 \\ -1.918931146 & -1.614122610 & -1.904704744 \\ -0.934291306 & -4.005261132 & -1.754978355 \\ -0.262854903 & -2.228133231 & -0.508282668 \end{vmatrix}$$

And for the denominator ($m = n - 1 = 2$)

$$\underline{\underline{C}}^{(2)T} = \begin{vmatrix} 1.000000000 & 1.000000000 & 1.000000000 \\ -0.244001948 & 0.365652907 & -1.068512526 \\ -0.574150861 & 1.385725477 & -0.771356469 \\ -0.432097367 & -1.359687152 & 0.067386858 \\ -0.895226091 & -2.866357848 & 0.206908269 \\ -0.462709527 & -1.518996192 & -0.248999874 \end{vmatrix}$$

iv) Quartic Orthotropic Fitted Closures ($n = 4$)

The constant coefficient matrix $\underline{\underline{C}}'$ based on regression analysis by Verweyst [40] developed from Carlson elliptic integrals.

$$\underline{\underline{C}}^{(4)T} = \begin{vmatrix} 0.6363 & 0.6363 & 2.7405 \\ -1.8727 & -3.3153 & -9.1220 \\ -4.4797 & -3.0371 & -12.2571 \\ 11.9590 & 11.8273 & 34.3199 \\ 3.8446 & 6.8815 & 13.8295 \\ 11.3421 & 8.4368 & 25.8685 \\ -10.9583 & -15.9121 & -37.7029 \\ -20.7278 & -15.1516 & -50.2756 \\ -2.1162 & -6.4873 & -10.8802 \\ -12.3876 & -8.6389 & -26.9637 \\ 9.8160 & 9.3252 & 27.3347 \\ 3.4790 & 7.7468 & 15.2651 \\ 11.7493 & 7.4815 & 26.1135 \\ 0.5080 & 2.2848 & 3.4321 \\ 4.8837 & 3.5977 & 10.6117 \end{vmatrix}$$

The constant coefficient matrix $\underline{\underline{C}}'$ based on regression analysis for the FFLAR4 closure by Mullens [42]

$$\underline{\underline{C}}^{(4)T} = \begin{vmatrix} 0.678225884 & 0.748226727 & 3.167356369 \\ -3.834359034 & -4.249612053 & -13.288266400 \\ -2.664862865 & -2.987266447 & -11.680179330 \\ 9.746185193 & 8.641488072 & 23.788431340 \\ 14.209962670 & 14.938209410 & 43.700607680 \\ 2.700369681 & 5.974489008 & 17.383121430 \\ -8.013024236 & -7.521216405 & -19.959054610 \\ -22.447252700 & -21.757217160 & -58.354308000 \\ -13.078649640 & -15.798676320 & -49.513705640 \\ -0.125467689 & -3.616551654 & -11.755525930 \end{vmatrix}$$

2.417857515	2.376441613	6.291273472
10.563248410	10.222185780	25.844317920
12.689484570	12.640352670	35.425354130
2.487386515	4.788201652	18.226443930
-0.328195677	1.056519961	2.925785795

The constant coefficient matrix $\underline{\underline{C}}'$ based on regression analysis for the LAR4 closure by Mullens [42] is

$$[\underline{\underline{C}}^{(4)}]^T = \begin{array}{|c|} \hline \begin{array}{ccc} 0.813175172 & 1.768619587 & 4.525066937 \\ -3.065410883 & -9.826017151 & -19.259137620 \\ -4.659333003 & -6.484058476 & -17.650178090 \\ 6.329870878 & 19.986994700 & 33.901239610 \\ 14.747639770 & 28.905936750 & 61.543979540 \\ 9.739797775 & 10.759963010 & 28.467355970 \\ -4.216519964 & -17.715409270 & -27.768082700 \\ -15.922240910 & -40.492387100 & -76.738638810 \\ -20.818571900 & -27.442217500 & -68.977583290 \\ -8.993993112 & -7.230748101 & -22.399036130 \\ 1.138888034 & 5.785725498 & 8.600822308 \\ 5.834142985 & 18.709047480 & 32.480679940 \\ 11.470974520 & 19.729631240 & 43.875135630 \\ 9.874209286 & 8.882877701 & 26.928320210 \\ 3.100457733 & 2.224834058 & 7.101978254 \end{array} \\ \hline \end{array}$$

c) Invariant Based Optimal Fitting Closure (IBOF) Approximation

The unknown coefficients of the binomial expansion for the six parameters in the IBOF closure representation based on regression fitting by Chung et al [44] of actual flow data obtained from the distribution function closure are given in Table 17 below.

$k \backslash m$	1	2	3
0	2.49409081657860E+01	-4.97217790110754E-01	2.34146291570999E+01
1	-4.35101153160329E+02	2.34980797511405E+01	-4.12048043372534E+02
2	7.03443657916476E+03	1.53965820593506E+02	5.73259594331015E+03
3	3.72389335663877E+03	-3.91044251397838E+02	3.19553200392089E+03
4	-1.33931929894245E+05	-2.13755248785646E+03	-6.05006113515592E+04
5	8.23995187366106E+05	1.52772950743819E+05	-4.85212803064813E+04
6	-1.59392396237307E+04	2.96004865275814E+03	-1.10656935176569E+04
7	8.80683515327916E+05	-4.00138947092812E+03	-4.77173740017567E+04
8	-9.91630690741981E+06	-1.85949305922308E+06	5.99066486689836E+06
9	8.00970026849796E+06	2.47717810054366E+06	-4.60543580680696E+07
10	3.22219416256417E+04	-1.04092072189767E+04	1.28967058686204E+04
11	-2.37010458689252E+06	1.01013983339062E+05	2.03042960322874E+06
12	3.79010599355267E+07	7.32341494213578E+06	-5.56606156734835E+07
13	-3.37010820273821E+07	-1.47919027644202E+07	5.67424911007837E+08
14	-2.57258805870567E+08	-6.35149929624336E+07	-1.52752854956514E+09
15	-2.32153488525298E+04	1.38088690964946E+04	4.66767581292985E+03
16	2.14419090344474E+06	-2.47435106210237E+05	-4.99321746092534E+06
17	-4.49275591851490E+07	-9.02980378929272E+06	1.32124828143333E+08
18	-2.13133920223355E+07	7.24969796807399E+06	-1.62359994620983E+09
19	1.57076702372204E+09	4.87093452892595E+08	7.92526849882218E+09
20	-3.95769398304473E+09	-1.60162178614234E+09	-1.28050778279459E+10

Table 17: 5th order binomial fitting coefficients for the IBOF closure approximation

Appendix III. The Center Gated Disk Flow Problem

For this flow the velocity gradient is not constant but varies with time or radial distance. There is thus an additional unknown r which is the radius where the 2nd order tensor achieves steady state. We thus need to find the partial derivative of the evolution equation with respect to r in addition to the independent components of the tensor which was previously obtained. The radial velocity in dimensionless form for this flow field is given by.

$$\tilde{v}_r = \frac{1}{\tilde{r}} [1 - \tilde{z}^2] \quad 142$$

Where \tilde{r} and \tilde{z} are the dimensionless radial and vertical distance given by $\tilde{r} = r/h$ & $\tilde{z} = z/h$ respectively. The actual velocity components are $v_r = \bar{v}\tilde{v}_r$, $v_\theta = v_z = 0$, where \bar{v} is the average velocity given as

$$\bar{v} = \frac{3Q}{8\pi h^2} \quad 143$$

The velocity gradient in dimensionless and non-dimensionless forms is thus given as (cf. Altan & Rao [54])

$$\tilde{L}_{ij} = \begin{bmatrix} -\frac{\tilde{v}_r}{\tilde{r}} & -2\frac{\tilde{z}}{\tilde{r}} \\ \frac{\tilde{v}_r}{\tilde{r}} & - \\ & - \end{bmatrix}, \quad L_{ij} = \frac{\bar{v}}{h} \tilde{L}_{ij} \quad 144$$

And the partial derivative of the velocity gradient with respect to the radial distance is given as

$$\frac{\partial \tilde{L}_{ij}}{\partial \tilde{r}} = -\frac{2}{\tilde{r}} \begin{bmatrix} -\frac{\tilde{v}_r}{\tilde{r}} & -\frac{\tilde{z}}{\tilde{r}} \\ \frac{\tilde{v}_r}{\tilde{r}} & - \\ & - \end{bmatrix}, \quad \frac{\partial L_{ij}}{\partial r} = \frac{\bar{v}}{h^2} \frac{\partial \tilde{L}_{ij}}{\partial \tilde{r}} \quad 145$$

The partial derivative of the vorticity tensor and the rate of deformation tensor with respect to the radial distance can thus be obtained from

$$\frac{\partial \omega_{ij}}{\partial r} = \frac{1}{2} \left[\frac{\partial L_{ij}}{\partial r} - \frac{\partial L_{ji}}{\partial r} \right], \quad \frac{\partial \dot{\gamma}_{ij}}{\partial r} = \frac{1}{2} \left[\frac{\partial L_{ij}}{\partial r} + \frac{\partial L_{ji}}{\partial r} \right] \quad 146$$

We can thus obtain the partial derivative of the material derivative of the 2nd order orientation tensor with respect to the radial distance for the various moment-tensor models described in preceding sections. All variables retain their usual definition.

Folgar-Tuckers (FT) Model

$$J_{r mn}^{FT} = \frac{\partial \dot{a}_{mn}^{FT}}{\partial r} = \frac{\partial \dot{a}_{mn}^{HD}}{\partial r} + \frac{\partial \dot{a}_{mn}^{IRD}}{\partial r} \quad 147$$

$$\frac{\partial \dot{a}_{mn}^{HD}}{\partial r} = - \left(\frac{\partial \omega_{mk}}{\partial r} a_{kn} - a_{mk} \frac{\partial \omega_{kn}}{\partial r} \right) + \xi \left(\frac{\partial \dot{\gamma}_{mk}}{\partial r} a_{kn} + a_{mk} \frac{\partial \dot{\gamma}_{kn}}{\partial r} - 2 \frac{\partial \dot{\gamma}_{kl}}{\partial r} a_{mnkl} \right) \quad 148$$

$$\frac{\partial \dot{a}_{mn}^{IRD}}{\partial r} = 2 \frac{\partial D_r}{\partial r} (\delta_{ij} - \alpha a_{ij}) \quad 149$$

$$\frac{\partial D_r}{\partial r} = C_l \frac{\partial \dot{\gamma}}{\partial r}, \quad \frac{\partial \dot{\gamma}}{\partial r} = \frac{2}{\dot{\gamma}} \left(\dot{\gamma}_{ij} \frac{\partial \dot{\gamma}_{ji}}{\partial r} \right) \quad 150$$

Reduced Strain Closure (RSC) Model

$$J_{r mn}^{RSC} = J_{r mn}^{FT} - (1 - \kappa) \frac{\partial \dot{a}_{mn}^{\Delta FT}}{\partial r} \quad 151$$

$$\frac{\partial \dot{a}_{mn}^{\Delta FT}}{\partial r} = 2\xi \frac{\partial \dot{\gamma}_{kl}}{\partial r} \{L_{mnkl} - M_{mnrs} a_{rskl}\} + \frac{\partial \dot{a}_{mn}^{IRD}}{\partial r} \quad 152$$

Phelps-Tucker ARD Model

$$J_{r mn}^{PT} = \frac{\partial \dot{a}_{mn}^{PT}}{\partial r} = \frac{\partial \dot{a}_{mn}^{HD}}{\partial r} + \frac{\partial \dot{a}_{mn}^{ARD}}{\partial r} \quad 153$$

where,

$$\frac{\partial \dot{a}_{mn}^{ARD}}{\partial r} = \dot{a}_{mn}^{ARD} \frac{1}{\dot{\gamma}} \frac{\partial \dot{\gamma}}{\partial r} + \dot{\gamma} \left[2 \frac{\partial C_{mn}}{\partial r} - 2 \frac{\partial C_{rs}}{\partial r} \delta_{rs} a_{mn} - 5 \left(\frac{\partial C_{mk}}{\partial r} a_{kn} + a_{mk} \frac{\partial C_{kn}}{\partial r} \right) + 10 a_{mnkl} \frac{\partial C_{kl}}{\partial r} \right] \quad 154$$

Moldflow ARD (MRD) Model

$$\dot{a}_{mn}^{mARD} = \dot{\gamma} [2C_{mn} - 2C_{kl} \delta_{kl} a_{mn}] \quad 155$$

$$\frac{\partial \dot{a}_{mn}^{mARD}}{\partial a_{ij}} = \dot{a}_{mn}^{mARD} \frac{1}{\dot{\gamma}} \frac{\partial \dot{\gamma}}{\partial r} + \dot{\gamma} \left[2 \frac{\partial C_{mn}}{\partial r} - 2 \frac{\partial C_{kl}}{\partial r} \delta_{kl} a_{mn} \right] \quad 156$$

The derivative of the spatial diffusion coefficients C_{mn} with respect to radial distance is also computed based on the applicable method listed below.

Phelps-Tucker ARD Model

$$\frac{\partial C_{mn}^{PT}}{\partial r} = \frac{b_4}{\dot{\gamma}^2} \left[\dot{\gamma} \frac{\partial \dot{\gamma}_{mn}}{\partial r} - \frac{\partial \dot{\gamma}}{\partial r} \dot{\gamma}_{mn} \right] + \frac{b_5}{\dot{\gamma}^3} \left[\left(\dot{\gamma} \frac{\partial \dot{\gamma}_{mk}}{\partial r} - \frac{\partial \dot{\gamma}}{\partial r} \dot{\gamma}_{mk} \right) \dot{\gamma}_{nk} + \dot{\gamma}_{mk} \left(\dot{\gamma} \frac{\partial \dot{\gamma}_{nk}}{\partial r} - \frac{\partial \dot{\gamma}}{\partial r} \dot{\gamma}_{nk} \right) \right] \quad 157$$

Tseng's improved ARD (iARD) Model

$$\frac{\partial C_{mn}^{iARD}}{\partial \tilde{r}} = -4C_I C_M \frac{1}{\dot{\gamma}^3} \left[\left(\dot{\gamma} \frac{\partial \dot{\gamma}_{mk}}{\partial r} - \frac{\partial \dot{\gamma}}{\partial r} \dot{\gamma}_{mk} \right) \dot{\gamma}_{nk} + \dot{\gamma}_{mk} \left(\dot{\gamma} \frac{\partial \dot{\gamma}_{nk}}{\partial r} - \frac{\partial \dot{\gamma}}{\partial r} \dot{\gamma}_{nk} \right) \right] \quad 158$$

Or

$$\frac{\partial C_{mn}^{iARD}}{\partial r} = -C_I C_M \frac{\partial \tilde{L}_{mn}}{\partial r}, \quad \frac{\partial \tilde{L}_{mn}}{\partial r} = \frac{1}{L_{rs} L_{rs}} \left[L_{mk} \frac{\partial L_{nk}}{\partial r} + \frac{\partial L_{mk}}{\partial r} L_{nk} - 2L_{rs} \frac{\partial L_{rs}}{\partial r} \tilde{L}_{mn} \right] \quad 159$$

For principal ARD ($pARD$), Wang's PT (WPT), and Dz models,

$$\frac{\partial C_{mn}^{iARD}}{\partial \tilde{r}} = \frac{\partial C_{mn}^{WPT}}{\partial \tilde{r}} = \frac{\partial C_{mn}^{Dz}}{\partial \tilde{r}} = 0 \quad 160$$

The material derivative can be expressed in Eulerian form thus.

$$\dot{a}_{mn}^{FT} = \frac{Da_{mn}}{Dt} = \frac{\partial a_{mn}}{\partial t} + v_k \frac{\partial a_{mn}}{\partial x_k} \quad 161$$

Or in radial coordinate

$$\dot{a}_{mn}^{FT} = \frac{Da_{mn}}{Dt} = \frac{\partial a_{mn}}{\partial t} + v_r \frac{\partial a_{mn}}{\partial r} + v_\theta \frac{1}{r} \frac{\partial a_{mn}}{\partial \theta} + v_z \frac{\partial a_{mn}}{\partial z} \quad 162$$

But $v_\theta = v_z = 0$ and the flow is steady i.e. $\partial()/\partial t = 0$, and $\partial()/\partial \theta = 0$ which simplifies eqn. 162 to

$$v_r \frac{\partial a_{mn}}{\partial r} = \dot{a}_{mn}^{FT} \quad 163$$

The residual is thus.

$$\hat{R}_{mn} = \frac{\partial a_{mn}}{\partial r} = \frac{\dot{a}_{mn}^{FT}}{v_r} \quad 164$$

And the Jacobian with respect to r and the components of the 2nd order tensor modified in this way becomes.

$$\hat{J}_{r_{mn}} = \frac{1}{v_r} \left[J_{r_{mn}} + \frac{\dot{a}_{mn}^{FT}}{r} \right], \quad \hat{J}_{m_{nij}} = \frac{J_{m_{nij}}}{v_r} \quad 165$$

$\hat{J}_{r_{mn}}^X$ can be represented in vector form as $\hat{J}_{r_i}^X$. The modified Jacobian J_{2ij}^X is thus a 5×6 matrix and the residual R_i^X is a 5×1 vector as previously obtained. i.e.,

$$\underline{J}_2^X = \begin{bmatrix} \hat{J}_{r_i}^X & \hat{J}_{m_{ij}}^X \end{bmatrix} \quad 166$$

It is evident that the above Jacobian is rank deficient, and we thus require an extra equation in form of a normalization condition to resolve this deficiency. We choose the Euclidean norm as the additional residual term and derive its associated derivative. i.e.

$$\hat{R}^X = \|\underline{\hat{R}}^X\|_2 = \sqrt{\sum_i [\hat{R}_i^X]^2}, \quad \hat{J}_j^X = \frac{1}{\|\underline{\hat{R}}^X\|_2} (\hat{R}_i^X J_{2ij}^X) \quad 167$$

Or for an n th norm

$$\hat{R}^X = \|\underline{\hat{R}}^X\|_n = \sqrt[n]{\sum_i [\hat{R}_i^X]^n}, \quad \hat{J}_j^X = \frac{1}{\{\|\underline{\hat{R}}^X\|_n\}^{(n-1)}} (\{\hat{R}_i^X\}^{(n-1)} J_{2ij}^X) \quad 168$$

The final forms of the residual \underline{R}_F^{FT} and the Jacobian \underline{J}_F^{FT} are thus.

$$\underline{R}_F^X = \begin{bmatrix} \hat{R}^X \\ \underline{\hat{R}}^X \end{bmatrix}, \quad \underline{J}_F^X = \begin{bmatrix} \hat{J}_j^X \\ \underline{J}_2^X \end{bmatrix} \quad 169$$

To avoid potential numerical instability that would arise due to the inherent singularity of the Jacobian at large radial distances, the diagonal of the Jacobian is slightly modified with a damping coefficient λ_F to ensure negative definitiveness of the matrix (cf. Phelps et al. [12]) i.e.

$$\underline{J}_F^X = \underline{J}_F^X - \lambda_F I \quad 170$$

Acknowledgement

Special Thanks to National Science Foundation for providing the necessary grants that made this publication possible and to Daniel Bourgeois who was very supportive throughout the duration in compilation of this Journal Paper

References

1. Jeffery, G.B., 1922. The motion of ellipsoidal particles immersed in a viscous fluid. *Proceedings of the Royal Society of London. Series A, Containing papers of a mathematical and physical character*, 102(715), pp.161-179.
2. Saffman, P.G., 1956. On the motion of small spheroidal particles in a viscous liquid. *Journal of Fluid Mechanics*, 1(5), pp.540-553.
3. Folgar, F. and Tucker III, C.L., 1984. Orientation behavior of fibers in concentrated suspensions. *Journal of reinforced plastics and composites*, 3(2), pp.98-119.
4. Portillo, F.F., 1983. *Fiber Orientation Distribution in Concentrated Suspensions: A Predictive Model*. University of Illinois at Urbana-Champaign.
5. Bay, R. S. (1991). Fiber orientation in injection-molded composites: a comparison of theory and experiment. University of Illinois at Urbana-Champaign.
6. Montgomery-Smith, S., Jack, D. and Smith, D.E., 2011. The fast exact closure for Jeffery's equation with diffusion. *Journal of Non-Newtonian Fluid Mechanics*, 166(7-8), pp.343-353.
7. Advani, S.G. and Tucker III, C.L., 1987. The use of tensors to describe and predict fiber orientation in short fiber composites. *Journal of rheology*, 31(8), pp.751-784.
8. Huynh, H.M., 2001. *Improved fiber orientation predictions for injection-molded composites* (Doctoral dissertation, University of Illinois at Urbana-Champaign).
9. Wang, J., O'Gara, J.F. and Tucker III, C.L., 2008. An objective model for slow orientation kinetics in concentrated fiber suspensions: Theory and rheological evidence. *Journal of Rheology*, 52(5), pp.1179-1200.
10. Tseng, H.C., Chang, R.Y. and Hsu, C.H., 2013. Phenomenological improvements to predictive models of fiber orientation in concentrated suspensions. *Journal of Rheology*, 57(6), pp.1597-1631.
11. Tseng, H.C., Chang, R.Y. and Hsu, C.H., Molecular Dynamics Tech Co Ltd and Coretech Systems Co Ltd, 2013. Method and computer readable media for determining orientation of fibers in a fluid. U.S. Patent 8,571,828.
12. Phelps, J.H. and Tucker III, C.L., 2009. An anisotropic rotary diffusion model for fiber orientation in short-and long-fiber thermoplastics. *Journal of Non-Newtonian Fluid Mechanics*, 156(3), pp.165-176.
13. Ranganathan, S. and Advani, S.G., 1991. Fiber-fiber interactions in homogeneous flows of non-dilute suspensions. *Journal of Rheology*, 35(8), pp.1499-1522.
14. Fan, X., Phan-Thien, N. and Zheng, R., 1998. A direct simulation of fibre suspensions. *Journal of Non-Newtonian Fluid Mechanics*, 74(1-3), pp.113-135.
15. Phan-Thien, N., Fan, X.J., Tanner, R.I. and Zheng, R., 2002. Folgar-Tucker constant for a fibre suspension in a Newtonian fluid. *Journal of Non-Newtonian Fluid Mechanics*, 103(2-3), pp.251-260.
16. Koch, D.L., 1995. A model for orientational diffusion in fiber suspensions. *Physics of Fluids*, 7(8), pp.2086-2088.
17. Hand, G.L., 1962. A theory of anisotropic fluids. *Journal of Fluid Mechanics*, 13(1), pp.33-46.
18. Tseng, H.C., Chang, R.Y. and Hsu, C.H., 2016. An objective tensor to predict anisotropic fiber orientation in concentrated suspensions. *Journal of Rheology*, 60(2), pp.215-224.
19. Tseng, H.C., Chang, R.Y. and Hsu, C.H., 2018. The use of principal spatial tensor to predict anisotropic fiber orientation in concentrated fiber suspensions. *Journal of Rheology*, 62(1), pp.313-320.
20. Bakharev, A., Yu, H., Ray, S., Speight, R. and Wang, J., 2018. Using new anisotropic rotational diffusion model to improve prediction of short fibers in thermoplastic injection molding. *Society of Plastics Engineers: Lubbock, TX, USA*.
21. Latz, A., Strautins, U. and Niedziela, D., 2010. Comparative numerical study of two concentrated fiber suspension models. *Journal of non-newtonian fluid mechanics*, 165(13-14), pp.764-781.

22. Kugler, S.K., Kech, A., Cruz, C. and Osswald, T., 2020. Fiber orientation predictions—a review of existing models. *Journal of Composites Science*, 4(2), p.69.
23. Favaloro, A.J. and Tucker III, C.L., 2019. Analysis of anisotropic rotary diffusion models for fiber orientation. *Composites Part A: Applied Science and Manufacturing*, 126, p.105605.
24. Agboola, B.O., Jack, D.A. and Montgomery-Smith, S., 2012. Effectiveness of recent fiber-interaction diffusion models for orientation and the part stiffness predictions in injection molded short-fiber reinforced composites. *Composites Part A: Applied Science and Manufacturing*, 43(11), pp.1959-1970.
25. Park, J.M. and Park, S.J., 2011. Modeling and simulation of fiber orientation in injection molding of polymer composites. *Mathematical Problems in Engineering*, 2011.
26. Bay, R.S. and Tucker III, C.L., 1992. Fiber orientation in simple injection moldings. Part I: Theory and numerical methods. *Polymer composites*, 13(4), pp.317-331.
27. Bay, R.S. and Tucker III, C.L., 1992. Fiber orientation in simple injection moldings. Part II: Experimental results. *Polymer composites*, 13(4), pp.332-341.
28. Gupta, M. and Wang, K.K., 1993. Fiber orientation and mechanical properties of short-fiber-reinforced injection-molded composites: Simulated and experimental results. *Polymer Composites*, 14(5), pp.367-382.
29. Chung, S.T. and Kwon, T.H., 1996. Coupled analysis of injection molding filling and fiber orientation, including in-plane velocity gradient effect. *Polymer Composites*, 17(6), pp.859-872.
30. Vincent, M., Devillers, E. and Agassant, J.F., 1997. Fibre orientation calculation in injection moulding of reinforced thermoplastics. *Journal of Non-Newtonian Fluid Mechanics*, 73(3), pp.317-326.
31. Vincent, M., Giroud, T., Clarke, A. and Eberhardt, C., 2005. Description and modeling of fiber orientation in injection molding of fiber reinforced thermoplastics. *Polymer*, 46(17), pp.6719-6725.
32. VerWeyst, B.E., Tucker, C.L., Foss, P.H. and O'Gara, J.F., 1999. Fiber orientation in 3-D injection molded features. *International Polymer Processing*, 14(4), pp.409-420.
33. Doi, M., 1981. Molecular dynamics and rheological properties of concentrated solutions of rodlike polymers in isotropic and liquid crystalline phases. *Journal of Polymer Science: Polymer Physics Edition*, 19(2), pp.229-243.
34. Lipscomb II, G.G., Denn, M.M., Hur, D.U. and Boger, D.V., 1988. The flow of fiber suspensions in complex geometries. *Journal of Non-Newtonian Fluid Mechanics*, 26(3), pp.297-325.
35. Hinch, E.J. and Leal, L.G., 1976. Constitutive equations in suspension mechanics. Part 2. Approximate forms for a suspension of rigid particles affected by Brownian rotations. *Journal of Fluid Mechanics*, 76(1), pp.187-208.
36. Cintra Jr, J.S. and Tucker III, C.L., 1995. Orthotropic closure approximations for flow-induced fiber orientation. *Journal of Rheology*, 39(6), pp.1095-1122.
37. Chung, D.H. and Kwon, T.H., 2000. Applications of recently proposed closure approximations to injection molding filling simulation of short-fiber reinforced plastics. *Korea-Australia Rheology Journal*, 12(2), pp.125-133.
38. Chung, D.H. and Kwon, T.H., 2001. Improved model of orthotropic closure approximation for flow induced fiber orientation. *Polymer composites*, 22(5), pp.636-649.
39. Kuzmin, D., 2018. Planar and orthotropic closures for orientation tensors in fiber suspension flow models. *SIAM Journal on Applied Mathematics*, 78(6), pp.3040-3059.
40. VerWeyst, B.E., 1998. Numerical predictions of flow-induced fiber orientation in three-dimensional geometries. University of Illinois at Urbana-Champaign.
41. Wetzel, E.D. and Tucker III, C.L., 1999. Area tensors for modeling microstructure during laminar liquid-liquid mixing. *International journal of multiphase flow*, 25(1), pp.35-61.
42. Mullens, M., 2010. Developing new fitted closure approximations for short-fiber reinforced polymer composites (Doctoral dissertation, University of Missouri--Columbia).

43. Verleye, V., Coumiot, A. and Dupret, F., 1970. Numerical prediction of fibre orientation in complex injection-moulded parts. *WIT Transactions on Engineering Sciences*, 4.
44. Chung, D.H. and Kwon, T.H., 2002. Invariant-based optimal fitting closure approximation for the numerical prediction of flow-induced fiber orientation. *Journal of rheology*, 46(1), pp.169-194.
45. Jack, D.A., Schache, B. and Smith, D.E., 2010. Neural network-based closure for modeling short-fiber suspensions. *Polymer Composites*, 31(7), pp.1125-1141.
46. Jack, D.A., 2003. Investigating the Use of Tensors in Numerical Prediction for Short-fiber Reinforced Polymer Composites (Doctoral dissertation, University of Missouri-Columbia).
47. Jack, D.A., 2006. Advanced analysis of short-fiber polymer composite material behavior (Doctoral dissertation, University of Missouri--Columbia).
48. Chapra, S.C., 2005. *Applied Numerical Methods with MATLAB for Engineers and Scientists*. McGraw-Hill International Edition.
49. Eberle, A.P., Ortman, K. and Baird, D.G., 2011. Structure and rheology of fiber suspensions. *Applied Polymer Rheology: Polymeric Fluids with Industrial Applications*, pp.113-151.
50. Tucker III, C.L., 2022. Fundamentals of fiber orientation: Description, measurement and prediction. Carl Hanser Verlag GmbH Co KG.
51. Wang, J., 2018. Moldflow Research & Development - [7 R&D-Update - Jin Wang.pdf \(autodesk.net\)](#)
52. Smith, D.E. and Siddhi, V., 2006. Generalized approach for incorporating normalization conditions in design sensitivity analysis of eigenvectors. *AIAA journal*, 44(11), pp.2552-2561.
53. Nelson, R.B., 1976. Simplified calculation of eigenvector derivatives. *AIAA journal*, 14(9), pp.1201-1205.
54. Altan, M.C. and Rao, B.N., 1995. Closed-form solution for the orientation field in a center-gated disk. *Journal of Rheology*, 39(3), pp.581-599.
55. Dray, D., Gilormini, P. and Régnier, G., 2007. Comparison of several closure approximations for evaluating the thermoelastic properties of an injection molded short-fiber composite. *Composites Science and Technology*, 67(7-8), pp.1601-1610.
56. VerWeyst, B.E., Tucker, C.L., Foss, P.H. and O'Gara, J.F., 1999. Fiber orientation in 3-D injection molded features. *International Polymer Processing*, 14(4), pp.409-420.
57. Ferec, J., Mezi, D., Advani, S.G. and Ausias, G., 2020. Axisymmetric flow simulations of fiber suspensions as described by 3D probability distribution function. *Journal of Non-Newtonian Fluid Mechanics*, 284, p.104367.
58. Sayah, N. and Smith, D.E., 2022. Effect of Process Parameters on Void Distribution, Volume Fraction, and Sphericity within the Bead Microstructure of Large-Area Additive Manufacturing Polymer Composites. *Polymers*, 14(23), p.5107.